Modeling the Role of External Stresses on the Austenite-to-Bainite Phase Transformations in 51CrV4 Steel

by

Mehmet Can Uslu

A Thesis Submitted to the
Graduate School of Engineering
in Partial Fulfillment of the Requirements for
the Degree of

Master of Science
in
Mechanical Engineering

Koc University

June 2010

ABSTRACT

A new model is proposed successfully predicting the initiation and evolution of austenite-to-bainite phase transformation, specifically capturing the time-dependent transformation kinetics. In particular, the isothermal bainitic transformation in 51CrV4 steel was both experimentally observed for various constant stress conditions, and significant improvement was obtained in comparison to the existing models. Specifically, both the transformation kinetics and the resultant transformation strains can be simultaneously predicted utilizing the same variant based approach. Simulation results are in good agreement with the experiments, evidencing the success of the proposed model in describing the transformation phenomena in terms of kinetics and transformation plasticity. Furthermore, the proposed formulation provides a basis for incorporating variant-variant interactions and cementite formation in the residual austenite matrix.

ÖZET

Östenit-beynit faz değişiminin zamana bağlı gelişimini hesaplayabilen sayısal bir model geliştirilmiştir. Özellikle, 51CrV4 çeliği üzerinde yapılan deneylerde görülen malzeme üzerine uygulanan yüklerin izotermal faz değişimine etkisi sayısal model ile hesaplanabilmiştir. Önerilen yaklaşımda beynit fazının gelişme yönlerinin hesaba katılması ile beraber zamana bağlı faz değişimi, faz değişimi sonucu meydana gelen gerinimler ve mikroyapı tek bir model ile hesaplanabilmekedir. Model sonuçları ile deney sonuçları arasındaki uyum önerilen modelin doğruluğunu desteklemektedir. Mevcut model, faz değişimi sırasında meydana gelen mikroyapı etkileşimleri ile sementit oluşumu hesaplamalarına temel oluşturmaktadır.

ACKNOWLEDGEMENTS

First of all, I would like to express my respectful gratitude to my advisor, Dr. Demircan Canadinç, for his great academic supervision and further mentorship. His scientific approaches will always be remembered and deeply appreciated.

I am grateful to the valuable supervision of Prof. Dr.-Ing Hans-Jürgen Maier during my studies at the University of Paderborn. I also would like to thank to the members of his research group, specifically Felix, Thomas, Hans-Gerd, Sarah, Pira, Sergej and Simon for their friendship and support.

I would like to thank Dr. Murat Sözer, Dr. Erdem Alaca and Dr. Mehmet Sayar for their valuable contributions to my studies at Koc University.

Last, but not least, sincere thanks to my family. They were always with me with their love, trust and prays. This work is dedicated to them.

I greet all solid mechanics community, to people who with their high efforts had either big or small achievements, which deserve the same respect.

TABLE OF CONTENTS

LIST OF TABLES

LIST OF FIGURES

NOMENCLATURE

$\Delta F^{\gamma \rightarrow \gamma_1 + \alpha}$	Free energy change during the formation of ferrite with equilibrium partitioning of carbon to the retained austenite [Joule mol^{-1}].
F_1	Stored elastic strain energy per mole of Widmanstatten ferrite [Joule mol^{-1}].
F_2	Stored elastic strain energy per mole of bainite [Joule mol^{-1}].
ΔF_N	Minimum energy needed for the nucleation of a detectable amount of ferrite [Joule mol^{-1}].
$\Delta F^{\gamma \rightarrow \alpha}$	Free energy change for the formation of bainite with the same composition of austenite [Joule mol^{-1}].
ΔF_m	Maximum free energy change accompanying the formation of a nucleus [Joule mol^{-1}].
T	Temperature [Kelvin].
v	Pre-exponentional attempt frequency factor [s^{-1}].
ΔF^*	Activation energy [Joule mol^{-1}].
R	Universal gas constant [Joule $Kelvin^{-1}$ mol^{-1}]
Nu	Nucleation rate [s^{-1}].

B_S	Bainite formation start temperature [Kelvin].
F_{St}	Strain energy per unit volume [Joule m^{-3}].
σ	Interfacial energy per unit area [Joule m^{-2}].
Ws	Widmastatten ferrite formation start temperature [Kelvin].
I_{ws}	Nucleation rate at Ws temperature [s^{-1}].
K_1	Fitting parameter in bainitic nucleation theory.
K_2	Fitting parameter in bainitic nucleation theory [Joule mol^{-1}].
K_3	Fitting parameter in bainitic nucleation theory [Joule mol^{-1}].
a_α	Lattice parameter of the martensitic phase [nm].
a_γ	Lattice parameter of the austenitic phase [nm].
I	Identity matrix.
m	Magnitude of shape deformation upon transformation.
s	Shear strain on habit plane.

n	Dilatational strain on habit plane.
$\mathbf{p}_{\gamma}$	Unit normal of a habit plane in austenitic coordinate frame.
$\mathbf{d}_{\gamma}$	Displacement vector of an invariant plane strain in austenitic coordinate frame.
$\mathbf{P}_{\gamma Z}$	Deformation matrix in austenitic coordinate frame accompanying the formation of z^{th} bainitic variant.
$\mathbf{P}_{SZ}$	Deformation matrix of z^{th} bainitic variant in the specimen coordinate frame.
$\mathbf{R}$	Rotation matrix.
U_z	Interaction energy of z^{th} bainitic variant [Joule mol^{-1}].
$\boldsymbol{\sigma}_{ij}$	Applied stress tensor [Pa].
N	Number of the active bainitic variants.
S_{ijkl}	Eshelby tensor.
$\boldsymbol{\varepsilon}_{ij}^{TP}$	Transformation strain tensor of a grain.
$\boldsymbol{\varepsilon}_{ij}^{G}$	Constrained transformation strain tensor of a grain.
$\boldsymbol{\varepsilon}_{ij\text{-}z}$	Transformation strain tensor of z^{th} bainitic variant.

$\boldsymbol{\varepsilon_{ij}^{TR}}$	Total transformation strain tensor of the specimen.
ν	Poisson's ratio.
I_z	Nucleation rate of z^{th} bainitic variant [s^{-1}].
γ	Molar volume [$m^3\ mol^{-1}$].
O_B	Grain boundary area [m^2].
$O_{\beta,z,y}$	Real intersection area between the test plane and z^{th} bainitic variant [m^2].
$\Delta O_{\beta,z,y}$	Increment in the real intersection area [m^2].
$O^e_{\beta,z,y}$	Extended intersection area between the test plane and z^{th} bainitic variant [m^2].
$\Delta O^e_{\beta,z,y}$	Increment in the extended intersection area [m^2].
$E_{k,m,y}$	Change in the intersection area at the test plane during a certain time interval [m^2].
$V^e_{\beta,z}$	Extended volume of z^{th} bainitic variant [m^3].
$\Delta V^e_{\beta,z}$	Increment in the extended volume of z^{th} bainitic variant [m^3].
$V_{\beta,z}$	Real volume of z^{th} bainitic variant [m^3].

$\Delta V_{\beta,z}$	Increment in the real volume of z^{th} bainitic variant [m^3].
q^{max}	Maximum length of a bainitic sheaf [m].
S_U	Surface area of a bainitic subunit per unit volume [m^{-1}].
θ	Autocatalysis factor.
l_u	Length of a bainitic subunit [m].
$V_{\beta,z}$	Volumetric fraction of z^{th} bainitic variant.
q_k	Length of a bainitic sheaf [m].
Δq_k	Increment in the length of a bainitic sheaf. [m].
Δt_z	Time needed to have a nucleation of a new bainitic sub-unit [s].
Δt	Time increment [s].
ε_a	Axial transformation strain.
ε_d	Diametral transformation strain.

Chapter 1

INTRODUCTION

Steel, a material that can provide both high strength and good ductility, possesses properties which can be tailored by varying the process parameters, such as deformation stresses and strains, and temperature [1]. Specifically, in today's technology, novel steels can be designed depending on the needs of material properties, by understanding the nature of the solid-state phase transformations ongoing during the time-temperature-deformation paths of the production processes and the resultant characteristics of the material. In this aspect, the following will be a short introduction giving the application examples of bainitic and martensitic phase transformations in steels to obtain improved material properties. The achievements in understanding the theory of phase transformations in steels are extensively applied to industry with certain benefits, which shows the need for the theoretical models predicting the microstructure evolutions during certain production processes including thermomechanical treatments, in order to come up with materials of demanded mechanical properties and efficient low-cost production processes.

A full understanding of the microstructure evolution during the bainitic and martensitic phase transformations makes possible the generation of dual-phase steels (DPS), which consists of multiphase structures with retaining austenite [2]. The multiphase structure of the material with retained austenite bring good ductility with high strength due to the transformation induced plasticity effect– (TRIP) mechanically-induced martensitic transformation of the retained austenite in the system, where the thermo-mechanical treatments and the chemical composition of the material is specifically designed in order to have a retained austenite in the system [2]. Specifically, the formation of bainitic transformation makes possible the existence of austenite at room temperature, which is in fact a phase for higher temperatures [3]. In this aspect, considering the mechanical

properties of bainitic and martensitic dual phase steels, it is observed that the ductility of the bainitic steels may exceed martensitic steels, due to the higher fraction of retained austenite in the system, hence enhanced ductility.

Studies on DPS revealed much higher strength and ductility parameters due to their TRIP effect in comparison with the conventional steels used in industry, where a true stress of 1200 MPa is reached corresponding to a 0.27 true strain. The conventional steel values remain in the order of 500 MPa with a true strain interval of 0.15 [2]. With reference to the improved mechanical properties, the increase in the interest of industry to DPS may be attributed to its formability when compared with traditional high-strength, low alloy steels (HSLA), which lets the production of the complex shaped productions and higher capacity to absorb the crash energy [4]. Additionally, the lower weight of DPS also makes it useful for the aerospace industry [4].

The ductility and strength of materials are not necessarily proportional, where an increase in one of the properties may not result with an increase in the other one [5]. Considering the dual phase steels, the strength of the material can be related to the existing bainitic or martensitic phase, whereas the ductility is related to austenite [6]. It is observed experimentally that with increasing bainitic phase content the material strength is increased with a decrease in the ductility, whereas the reduction in bainitic content, hence an increment in the austenitic phase increased toughness with decreasing strength.

The only way to increase the strength and toughness simultaneously in a material is grain refinement [7]. This is due to the fact that as the scale of the microstructures in a material is decreased, the corresponding toughness and strength properties also improve [8]. An application of this phenomenon may be given with bainitic transformations [6], where the resultant small bainitic plates with a thickness of as small as 30 nm is achieved upon certain heat treatments and chemical composition modifications [9]. This kind of small scaled microstructures are determined by reducing the temperatures at which transformation takes place, and the reduction in the transformation temperature is possible

with understanding the transformation mechanisms and kinetics. The refinement in the microstructure also increases the hardness significantly, values exceeding 600 HV in [9]. The resultant steel produces a yield strength of 1.5 GPa, ultimate tensile strength up to 2.2 GPa and a ductility reaching %30 [6]. An example of its application may be the reduction in the wall thickness of pipelines, which is beneficial for welding processes [10].

Besides designing DPS with complex microstructures to obtain high strength and good ductility, controlling the effect of time-temperature path on phase transformations has applications in reducing the residual stresses in materials, such as in welding processes. Specifically, a certain tensile stress field is introduced in the constrained material after the decrease of the temperature to ambient temperature [11,12]. A new weld material designed has a remarkably low martensitic transformation temperature, where transformation starts around 180 °C and gets completed in the ambient temperature [11], and in this aspect, the introduction of the phase transformation during cooling, and especially at low temperatures eliminates the tensile residual stresses accumulating in the material with the volumetric expansion in the material due to the martensitic transformation. The volumetric expansion in the material due to the martensitic phase transformation compensates the tensile contraction strains in the material, and finally material comes up with compressive stress fields when system reaches the ambient temperature, which dramatically increases the fatigue life of the components [13]. At this point, it is important to predict the final microstructure of the material upon cooling under constant loadings and control the transformation strains occurring in order to compensate the thermal contraction strains introduced to the system due to welding.

Another field where a crucial need for understanding the effect of time-temperature-deformation paths on the final microstructure exits is the production of functional graded materials. A significant effort in this field is spent in order to develop modern production processes with the control of the evolution of the material microstructures through the production [1]. Considering a forging process, the high temperature and deformation

gradients introduced to the material during the phase transformation creates remarkable anisotropy and changes the local properties of the material [1]. The key idea here is that, if the evolution of the material anisotropy is controlled during the thermomechanical heat treatment, then functionally graded materials may be formed in only one production step, and production of a near-net-shape workpiece during forging would decrease the related production costs significantly, since only minor post processing like turning and milling is needed [14]. Considering the aim of producing a functionally graded material, with the introduced forging process, the thermomechanical treatments should lead to different microstructures within a single workpiece, and the final material properties should vary from location to location in the workpiece depending on the needs. This is the case for the products like gears, which are hard at the surface regions and tenacious in the inner parts [14]. During the process, the temperature gradients and the internal stresses existing in the material strongly affect the nature of the phase transformation kinetics. These effects should be predicted accurately in order to maintain the geometric stability of the material, since phase transformations cause certain distortions within the material with volume changes [14]. Then, a need for the full understanding of bainitic and martensitic transformation kinetics and the resultant material deformations and textures comes to picture, since they are the main phases at the final stage of the forging process in discuss.

With reference to the described application fields of the phase transformations in steels and the resultant benefits, it is crucial to understand the mechanism and kinetics of the transformation and be able to predict the final microstructure, in order to design steels with desired material properties. Extensive studies are performed in this aspect and significant processes are obtained, where it is possible to state that the current theory on steels is enough to determine novel alloys [13].

The aim of the current study is to develop a model in order to predict simultaneously the kinetics and the resulting transformation strains of an isothermal bainitic transformation under certain constant loadings. The proposed theory is based on the principles of the

previously proposed theories on the mechanism of bainitic transformation and texture evolution, which have relatively limited outputs compared with the current aim [15,16]. More specifically, with the applied modifications to be described in the following chapters, the ability of the proposed model to simultaneously calculate the transformation kinetics and transformation strains may be regarded as an improvement for the theory, with reference to the statements in the literature that the effect of stress on the bainitic transformations is a field which needs further developments with quantitative treatments [3].

The application of the model will demonstrate the resultant texture evolution and the transformation plasticity of certain bainitic steel upon the transformation, and additionally the shift in the transformation rate with respect to the introduced external loading will be calculated. The results will help to better understand the microstructure evolution and the resultant deformation of bainitic steels under certain thermal and mechanical treatments.

Stating the structure of the thesis, Chapter 2 gives a literature review on the nature of bainitic phase transformations. The nucleation and growth mechanisms are explained in detail, which further lead to the appearance of kinetics models to describe the evolution of bainitic phase under certain thermal and mechanical conditions. Later on, recent studies adapting the developed theories with certain modifications and predicting the transformation kinetics and transformation plasticity are given with their criticisms.

Chapter 3 gives the theoretical background of the proposed model. It initially describes the bainitic transformation crystallography and the resultant transformation strain calculations in microscale and macroscale. The interaction of the applied stresses with the transformation strains is explained. After that, the general transformation kinetics theory is described with the modifications done in order have a variant based model [15].

Chapter 4 deals with the experiments done in order to obtain the necessary data for the validation of the simulation results, where specific information about the material is

given with the process parameters governing the nature of the solid-state phase transformation. General information about the experimental setup is given.

Chapter 5 gives the simulation results and compares them with the experiment data. A detailed discussion is presented on the comparison of the experimental and numeric data, and the application of the model to the current system.

Chapter 6 gives the conclusion, summarizing the benefits of the model and describes the future work to be done for the possible improvements on the model.

Chapter 2

LITERATURE REVIEW

The discovery of bainite goes back to 1920s, where Davenport and Bain discovered a new microstructure with an “acicular, dark etching aggregates” at temperature levels above the martensitic transformation initiation and below the formation of pearlite [17,18]. The discovered microstructure was having higher toughness property compared with tempered martensite, and named as ‘Bainite’ in 1934, in honor of E.C. Bain [19-21].

It was initially proposed that the bainite transformation involved the formation of flat plates of supersatured ferrite with carbon, and later on the the distribution of carbon atoms at retaining austenite matrix, hence leading the formation of carbides [22,23]. The aggregates of ferritic plates were called as “sheaves”, and the plates in each sheaf were the sub-units [24,25].

In this aspect, one of the main debates in the literature was the determination of the mechanism for the formation of the ferritic components in steels, where two major theses were that the phase transformation emerged with either a displacive or a diffusion controlled mechanism [26-28].

A brief definition of the terms “displacive transformation” and “diffusion controlled transformation” shall be introduced here in order to make the story clearer. A displacive transformation is named for a transformation where individual atomic movements are less then one interatomic spacing. Due to the coordinated movements of the atoms during this transformation, it is termed as “military”. Diffusional

transformation, on the other hand, may be accompanied by the long-range diffusion of atoms within the material, termed as “civilian” [29].

The theory introduced with the displacive mechanism by Oblak and Heheman [26,27] was the growth of bainitic ferrite by the nucleation of discrete and successive plates of martensitic sub-units and the aggregate of these sub-units forming the sheaf structure. The nucleation of bainitic ferrite was treated as carbon-supersaturated with an immediate partitioning of the carbon into the residual austenite following the nucleation [26,27], whereas the reconstructive mechanism stated that the lengthening of the bainitic sheaves emerge with a diffusion controlled growth mechanism, by describing the ferritic sub-units as propagating ledges [26,28].

Following the debate on the nucleation mechanism on bainite, Bhadeshia introduced a study focusing on the microstructure of the transformed bainite, claiming that the growth had a displacive mechanism [26]. In this aspect, an earlier study already had experimental evidences that the nature of the growth mechanism should have a displacive manner [30], whereas the proposed study handled the growth mechanism in more detail, to justify the predicted displacive manner. The microstructure of the bainitic sheaf was examined with electron micrographs, and seen that the sheaves consisted of plate-shaped sub-units. The aggregation of the sub-units created a plate-like morphology and that the sub-units were in the same orientation with reference to grain and separated by films of retained austenite [26]. It was also observed from the micrographs that the nucleation of the sub-units occurred near the tips of the existing sub-units. Calculations were performed to obtain the temperature level where austenite and ferrite phases had the same free energies, hence in equilibrium, and a displacive transformation was possible below the specified temperature with a full saturation of carbon. The obtained temperature ranges for a various concentrations of carbon in the austenite and comparison of these results with the experimental data revealed the fact that the nucleation of ferritic bainite was accompanied by a small amount of carbon distribution

to the retained austenite, where the nucleated ferritic bainite was carbon supersaturated [26]. Following this observation, it was concluded that the diffusion of the carbon to the retained austenite occurred after the formation of ferritic bainite mostly. The observation of the incomplete reaction phenomenon in a previous study for Si-steel [30] was also described in this content, where bainitic reaction ceased at a certain point, and a full transformation of the microstructure to the bainite couldn't be achieved. The reason of this phenomenon was then attributed to the stabilization of the retained austenite with the introduction of the carbon atoms from the supersatured ferritic sub-units. Accordingly, the transformation stopped at a certain point since the carbon concentration in the austenitic matrix made the bainitic transformation energetically unfavorable. Figure 1 below gives the microstructure evolution during the bainitic transformation [31].

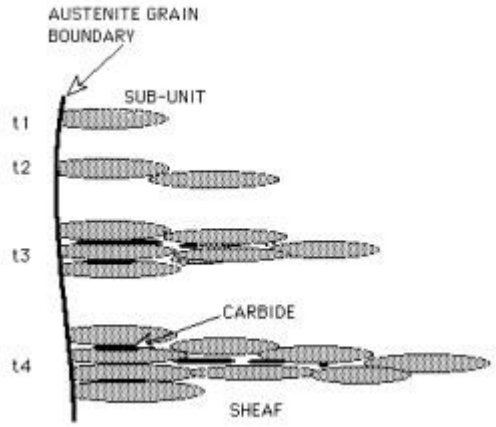

Figure 1: The microstructure evolution with time (t4 > t3 > t2 > t1) during bainitic transformation [31].

In a further experiment it was seen that, after the saturation of a bainitic transformation, holding the system at the isothermal transformation temperature for a remarkable time interval, almost a day, didn't increase the volumetric fraction of the bainitic ferrite, but interestingly the formation of diffusional transformation charactered pearlite was observed [26,30]. Consequently, the incomplete reaction phenomenon was

attributed to the displacive nucleation mechanism of the bainitic ferrite, since the diffusional transformation didn't stop [26]. Additional experimental studies also revealed the fact that the bainitic reaction start temperatures were low for the thermal activation of the diffusional transformation.

Another significant observation regarding the diffusion of extra carbon from the ferritic sub-units to the retained austenite was that, the diffused austenite wasn't homogenous in the retained austenite, and that the austenite films existing between the neighboring sub-units had higher concentrations [26]. This physically favored the nucleation of the new sub-units at the tips of the existing sub-units, since the carbon concentration was relatively low at the retained austenite compared with the films among the existing sub-units; hence less stabilized [26]. The limited size of the ferritic sub-units was also attributed to the plastic deformation of the austenite during the growth of bainitic ferrite, where the corresponding lattice distortion acted as a certain barrier to the further growth of the sub-units [26]. This phenomenon was recalled as a growth mechanism with an interface friction control [32].

On the growth mechanism of bainite [33], the experimental data collected regarding the growth rate of bainite sheaves were compared with the calculations based on the diffusion controlled paraequilibrium transformation, and it was seen that the experimental results always showed a higher growth rate of the bainitic sheaves when compared with the theoretical calculations based on diffusion growth. In this aspect, this difference was attributed to the displacive growth mechanism of bainite, and the later diffusion of the excessive carbon to the retained austenite.

Another study within the dates of the studies above by Bhadeshia [32] focused on the nucleation mechanisms and thermodynamics of two microstructures in steels, Widmanstatten ferrite and bainite. Following the free energy calculations needed to have a detectable nucleation of Widmanstatten ferrite and bainite, it was understood that the nucleation mechanisms of both structures involved the equilibrium partitioning of

carbon. The extend to decide whether a bainite or Widmanstatten ferrite would occur depended on the driving force available in the system, whether it was enough to support the growth of bainite with the super saturation of carbon, or had equilibrium partitioning of carbon with the growth of Widmanstatten ferrite [32]. In terms of thermodynamics, the transformation temperature to Widmanstatten ferrite was obtained by equating the strain energy of the formed phase to the chemical driving force available in the system for certain carbon concentrations. Following the equilibrium partitioning of carbon during the nucleation, it was seen that the free energy necessary to obtain a detectable amount of nucleation was linearly related with the displacive transformation start temperature [32].

Considering the diffusion controlled growth and nucleation of Widmanstatten ferrite, which corresponds to equilibrium partition of carbon, and the full carbon supersaturated growth mechanism of bainite with a diffusion controlled nucleation as Widmanstatten ferrite, the following nucleation and growth criteria were presented for both phases [32]:

The growth and nucleation criteria of Widmanstatten ferrite was described with

$$\left|\Delta F^{\gamma\rightarrow\gamma_1+\alpha}\right| > F_1 \quad (1)$$

$$\left|\Delta F^{\gamma\rightarrow\gamma_1+\alpha}\right| > \Delta F_N \quad (2)$$

In Equation (1), F_1 stands for the stored strain energy per mole of Widmanstatten ferrite. Equation (1) stands for the growth criteria, whereas Equation (2) stands for the nucleation criteria. ΔF_N stands for the minimum energy needed for a detectable amount of ferrite. $\Delta F^{\gamma\rightarrow\gamma_1+\alpha}$ corresponds to the free energy change during the phase transformation with equilibrium partitioning of carbon to the retained austenite. It is important in this context to realize one more time that, since both nucleation and growth mechanism of Widmanstatten ferrite involved the equilibrium partition of carbon to the

retained austenite, same free energy change was used in the nucleation and growth criteria in Equations (1) and (2); however, the situation wasn't the same for the bainitic reaction, which had a equilibrium partitioning of carbon for the nucleation mechanism, but formed supersatured ferrite during the growth process with no partition [26]. Accordingly, the growth and nucleation criteria for the bainite were given as

$$\left|\Delta F^{\gamma\rightarrow\alpha}\right| > F_2 \tag{3}$$

$$\left|\Delta F^{\gamma\rightarrow\gamma_1+\alpha}\right| > \Delta F_N \tag{4}$$

with F_2 defined as the stored elastic strain energy per mole of bainite and $\Delta F^{\gamma\rightarrow\alpha}$ free energy change with the formation of bainite with the same composition of austenite [32]. F_2 was determined to be about 400 J/mol [32].

In 1982, a further study was developed in order to calculate the isothermal transformation diagrams depending on the chemical composition of steels [34]. With the proposed model, the prediction of the time-temperature-transformation (TTT) curves was enabled for various steels. The curves were useful in order to predict the time necessary to have a certain amount of nucleation after the thermal treatments and the nature of the transformation, either displacive or diffusive at varying temperature ranges. The proposed model was useful in the design of desired steels upon certain heat treatments [34]. See Figure 2 below for illustration [35].

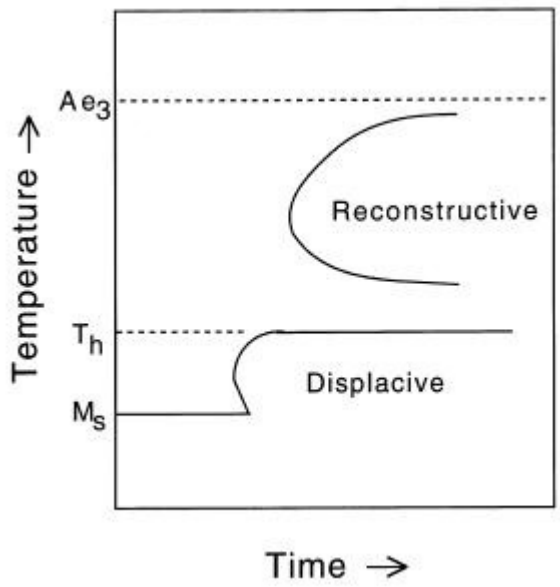

Figure 2: Schematic TTT diagram, illustrating the nature of the phase transformation with respect to temperature, and the time needed to obtain a certain amount of product phase. T_h indicates the highest temperature that ferrite can form by a displacive transformation [35].

During the theoretical considerations in order to develop a model to predict the TTT curves, a few improvements were made on the theory mentioned previously. The initial change was that, during the nucleation of the new phase, initially it was stated that the free energy change accompanying the nucleation shall be regarded as having equilibrium content of carbon atoms, defined as $\Delta F^{\gamma \rightarrow \gamma_1 + \alpha}$. However, recent study proposed the fact that, since during the nucleation the ferrite volume was quite small, quite low carbon content would diffuse. Accordingly, the free energy change accompanying the nucleation would be better defined with the term ΔF_m, which corresponded to the maximum free energy change accompanying the formation of a nucleus with a certain chemical composition. See Figure 3 below for illustration [34].

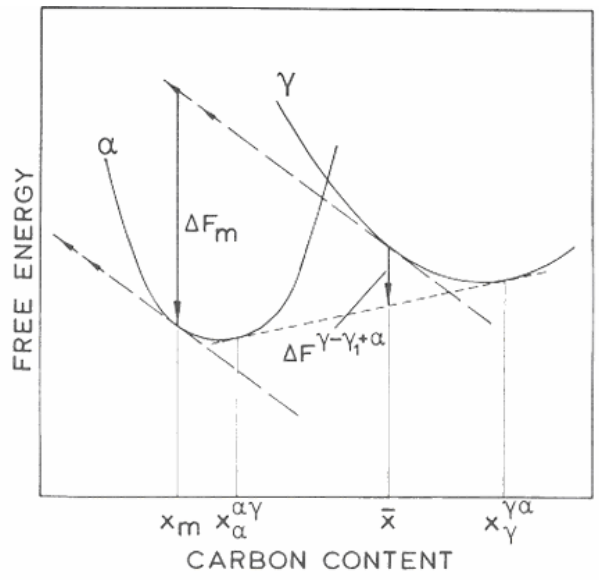

Figure 3: Scheme of the free energy changes during the nucleation and growth of ferrite [34].

Once obtaining the complete definition of the ferritic nucleation theory, the linear relation between the transformation start temperature, T and the amount of free energy needed in order to obtain a detectable nucleation rate ΔF_N was proposed with the formulation [36]

$$\Delta F_N = 3.637\,(T - 273) - 2540 \text{ J mol}^{-1} \quad (5)$$

The first theory on the kinetics of bainitic transformation was based on a transformation mechanism and proposed by Bhadeshia [37]. It had the statements that individual ferritic sub-units grew without the diffusion of carbon atoms, later partitioned the excess carbon to retained austenite and the size of each sub-unit was limited by the interface friction control mechanism [15,32]. The growth hence was ceased at a certain point where the driving force in the system wasn't high enough to overcome the frictional forces at the interface which was due to the distortion of the lattice with the plastic deformation [32]. The direct proportionality between the activation energy for the

nucleation of bainite and the driving force of transformation (chemical free energy) was utilized while determining the nucleation rate per unit volume during the bainitic transformation [37]. This relation was obtained with the derivations below, given by Bhadeshia [32], which is also the derivation of the relation given above in Equation (5).

It was stated in the general nucleation theory that the nucleation rate, Nu, may be determined with [32]

$$Nu \sim v \exp(-\Delta F^{*}/RT) \tag{6}$$

where

v = pre-exponentional attempt frequency factor

ΔF^{*} = activation barrier

R = gas constant

Equation (6) may be interpreted as

$$-\Delta F^{*} \sim RT \ln\left(\frac{N}{v}\right) \tag{7}$$

or shortly as

$$-\Delta F^{*} \sim \beta T. \tag{8}$$

$$\beta = R \ln\left(\frac{N}{v}\right) \tag{9}$$

where Nu, the detectable nucleation rate, was assumed to be constant and applicable to all steels at W_S, the temperature at which the displacive formation was first observed [32]. This in fact was the methodology followed to come up with a universal curve which expresses the minimum driving force necessary to obtain a detectable nucleation rate for any steel. This was forwarded as [32]

$$\Delta F^{*} = \lambda_1 \Delta F_{Bs}^{\gamma \rightarrow \gamma l + \alpha} + \lambda_1 F_{St} + \lambda_2 \sigma + \lambda_3 \tag{10}$$

where λ_{1-3} were constants, F_{St} was the strain energy per unit volume of the nucleus , σ was the interfacial energy per unit area and $\Delta F_{Bs}^{\gamma \rightarrow \gamma 1+\alpha}$ was the chemical free energy change of the nucleation for the equilibrium partition of carbon at the Bs temperature. Following Equation (6) and (10) then, the below relation was obtained [32]

$$-\lambda_1 \left| \Delta F_{Bs}^{\gamma \rightarrow \gamma 1+\alpha} \right| \sim |\beta| T - \lambda_1 |F_{St}| - \lambda_2 |\sigma| - \lambda_3 \quad (11)$$

which indicated the proportional relation between the free energy change necessary to obtain a detectable amount of nucleation and temperature. This relation provided the theoretical background for the assumption of a universal curve independent of the chemical composition of the steel used, which defined the minimum free energy change necessary to obtain a detectable amount of nucleation rate at the transformation start temperature, or in other words, with the given curve, the Ws temperature (Widmastatten ferrite formation start temperature) for a steel could be obtained [38]. The application of the theory was later also validated for high carbon steels [38].

The mathematical expression of the statement that the activation energy for the nucleation was a linear function of the chemical driving force available in the system was given by Equation (10), which when put in Equation (6) defined the nucleation rate in terms of the free energy change available in the system as [37]

$$I = v \exp\left(\frac{-C_2 + C_3 \Delta F_m}{RT} \right) \quad (12)$$

which was further manipulated to obtain nucleation rate at a certain temperature in terms of the nucleation rate at W_S temperature as [37]

$$I = I_{ws} \exp\left[\frac{-C_2 \Delta T}{R\, T\, Ws} - \frac{C_3}{R} \left(\frac{\Delta F_m}{T} - \frac{\Delta F_N}{Ws} \right) \right] \quad (13)$$

where T was the absolute temperature, R was the universal gas constant, $\Delta T = T - Ws$, C_2 and C_3 to be determined with fitting, and I_{ws} was the nucleation rate at Ws temperature.

At first sight, it is important to notice the usage of the term ΔF_m instead of $\Delta F_{Bs}^{\gamma \rightarrow \gamma 1+\alpha}$, that the maximum free energy available in the system was taken into account during the nucleation, where the reason of this phenomenon was described previously. It is also useful to mention one more that the amount of the energy between the two cases are similar to each other in anyway, but the application of the initial was assumed to be more correct in order to have a proper understanding and application of the nucleation theory [34].

Additional derivations to take into account the saturation of the austenitic matrix with carbon diffusion, the autocatalysis effect - the nucleation of the bainitic sub-units not only from the grain boundaries, but also from the tips of the new boundaries between the formed ferritic sub-units and retained austenite - aren't given here, since the derivations are quite complicated for the literature review part. Detailed derivations will be seen in the Theory part of the thesis. The meaning of Equation (12), which related the nucleation rate to the free energy available in the system is important and also enough to follow the improvements in the theory in the following years, since most modifications effecting the nature of the simulations in order to come up with better estimations of transformation kinetics were done on the relation between the free energy available in the system and the corresponding nucleation rate.

Further studies on the proposed kinetics theory revealed certain errors in predicting the isothermal transformation kinetics of bainitic transformation [39]. Specifically, the noticed problem was that, even though while generating the nucleation theory, it was assumed that all steels, independent of their chemical composition, had the same nucleation rate at their related W_S temperature, the results of the model yielded that steels with different compositions had different nucleation rates at their W_S temperature. This output was inconsistent with the theory, hence incorrect. The initial model had also prediction errors on the effect of undercooling and saturation of austenite with excess

carbon in ferritic sub-units to the transformation kinetics [39]. At this point, a new nucleation theory was developed to eliminate these difficulties, and especially determine a nucleation function which would reveal the same nucleation rates for the W_S temperatures of steels, independent of their chemical composition, consistent with the theory. The proposed model defined the nucleation rate of bainite as [39]

$$I = K_1 \exp\left(-\frac{K_2}{RT} - \frac{K_2 \Delta F_m}{rRT}\right) \tag{14}$$

with K_1 and K_2 were constants to be determined with fitting to the experimental data, of which K_1 represented the number of potential sites for nucleation, r was determined to be 2540 J mol^{-1} [36,39]. Additional formulations for the autocatalysis effect, saturation of austenite due to the carbon enrichment and the effect of grain size on the nucleation rate aren't given here for sake of simplicity. A detailed explanation will be defined in the Theory section. A following study proposed in this aspect dealed with the non-uniform carbon distribution in the austenite matrix [40]. It was seen that the carbon concentration in the austenitic films between the bainitic sheaves had a higher carbon concentration compared with the retaining austenite matrix, which accelerated the transformation, and also increased the maximum extend of the bainitic ferrite possible to form in a system [40].

Further improvements on the proposed model were done by Matsuda and Bhadeshia [15], where the initial nucleation events at the grain boundaries and the following nucleations with the autocatalysis process were modeled separately. This improvement gave a better understanding of grain boundary effect and the formation of the sheaves due to the autocatalysis processes [15]. The study also supplied a well defined theory, applicable to numerical studies, which was used in the kinetics calculations of the thesis. One of the benefits of the proposed study was that, it also reduced the number of fitting parameters.

Studies on the development of the bainitic transformation models later focused on the stress-kinetics and stress-texture relations, which is the path that the recent literature also followed. A study was presented by Bhadeshia, David, Vitek and Reed [41], regarding the transformation strains under various stress fields below the yield point of the austenitic phase. (It is important to distinguish the term “applied loading” and “stress field”, since the stresses existing in the material may be internal stresses, due to the phase transformations occurring in the material which causes certain distortions, or temperature drop and the resultant residual stresses, as in welding operations.) The resultant experimental images indicated the aligned bainitic plates in accordance with the stresses. The anisotropy in the resultant transformation strains, i.e. the difference between the axial and radial transformation strains were also observed to increase with the increase in the applied loadings [41]. The anisotropic transformation strains were attributed to the large shear component of the deformation during the bainitic transformation, which didn’t cancel in macroscale to produce an isotropic strain distribution. It is expected in a polycrystalline sample undergoing stress-free bainitic transformation to have an isotropic transformation strain distribution, since the random distribution of the bainitic variants would cancel the shear strains in macroscale.

In a study by Shipway and Bhadeshia [42], the transformation kinetics with the applied external loading was studied, and a remarkable increase in the transformation rate was observed as the applied load in the system was increased. It was noted during the experiments that as the transformation temperature increased, the effect of the applied external loadings on the transformation kinetics also increased, which was related to the lower chemical free energies available in the system at higher temperatures, hence a more remarkable effect of the mechanical driving force introduced to the system with the applied loadings. Transformation strain anisotropy was also observed in the experiments with the determination of transformation plasticity under various temperatures and loadings. This anisotropy can also be regarded as a proof that

the transformation has a displacive mechanism with a large shear component, since the shear component doesn't exist in the diffusion control reconstructive mechanisms [42].

An experimental study aimed to obtain the shear and dilatation magnitudes in the lattice during the transformation and determined a shear strain of 0.26 and a dilatational strain of 0.03 on the interface between the parent and product phases, where the details of the mechanism will be described in the Theory section [43]. Another important phenomena observed with the experiments was that, by using AFM tip and generating the surface topography, it was understood that the deformation due to the bainitic transformation was accommodated in the retaining austenite phase with plastic deformation [43]. This study, which focused in experiments and experimental imaging was important in terms of generating data in a quite small scale, to measure the related transformation strains. Experimental results also supported the general bainitic transformation mechanisms.

Bhadeshia [44] further carried the effect of the applied stresses on the transformation kinetic to the regime where the stress magnitudes were in excess of the yield point of the material. It was seen from optical microscopy views that the forest dislocations generated from the initial plastic deformation of the austenite grains before the transformation significantly reduced the size of the ferritic sub-units, since the forest dislocations acted as barriers for further nucleation. The extent of the transformation was then reduced due to the heavy deformation of the parent phase, which was recalled as mechanical stabilization [39]. It was also claimed within the study that, the plastic deformation of the parent phase may also increase the nucleation rate of the ferritic sub-units, since dislocations acted as additional nucleation sites; however, this effect was limited to a certain extend through the plastic deformation, where the dislocation density in the material reached a certain value.

The effect of stresses on the bainitic transformation kinetics was also studied by Lambers, Tschumak, Maier and Canadinc [14], where both the elastic stresses imposed

to the material during the transformation and plastic pre-straining of the material before the transformation was considered. It was seen that the application of elastic stresses and the plastic pre-deformation on the supercooled austenite at 340 C° increased the transformation plasticity. The increase in the transformation plasticity was attributed to the existence of internal stress fields upon the deformation, which favored certain bainitic variants to form. On the other hand, the plastic pre-deformation on the stable austenite at 1050 C° didn't lead to any transformation plasticity upon the transformation at 350 °C, opposite to expected. This was related to the fact that the internal stress fields generated during the plastic straining disappeared while cooling to the isothermal transformation temperature in order to initiate the transformation [14].

The increase in the transformation rate with the applied elastic stress was attributed to the higher nucleation rates, and also the formation of less active variants in the system, which yielded a less resistance to growth [14]. The effect of pre-straining, on the other hand, depended on the extent of the deformation. Even though it was stated previously that the formation of bainite was decelerated due to the increased dislocation density and the resulting obstacles [44], it was seen that the transformation rate was increased with the applied low pre-straining, due to the increased nucleation sites with the generation of dislocations, where the dislocation density became an important parameter in order to determine whether it would promote or resist the transformation. According to the experiment results, the effect of austenization also affected the transformation rate, where incomplete austenization promoted the kinetics in terms of the fact that existing of the carbides reduced the carbon content in the parent matrix, and also acted as additional nucleation sites for the transformation [14].

At this point, it is important to give the descriptions of stress-effected and strain induced transformations. In the former, the shape deformation accompanying the martensitic transformation interacts with the applied stresses; hence a mechanical driving force is introduced to the system in addition to the existing chemical free energy

available [45]. The latter is that, the dislocations generated during the plastic deformation of austenite increases the nucleation rate of the system by introducing new nucleation sites.

In their study, Hase, Garcia-Mateo and Bhadeshia [46] also studied the effect of applied stresses on the transformation kinetics and resultant texture. The results indicated that the applied stresses below the yield point of the material increased the rate of the transformation kinetics. The results also indicated that the effect of the mechanical driving force introduced to the system with the applied loadings increased with increasing temperatures. This was attributed to the fact that the chemical free energy available in the system decreased with increasing temperature, hence the mechanical driving force in the system became more effective as previously indicated by Shipway and Bhadeshia [42], but still smaller than the chemical free energy [46]. An important assumption made in this study was that, during the calculations in order to obtain the mechanical driving force, the maximum driving force resolved on the system was counted as the mechanical driving force available in the system, in order to compare with the chemical driving force available. This assumption was based on the study performed by Patel and Cohen [47], where the maximum driving force available in the system was calculated in order to obtain the shift in the martensitic transformation temperature. This shift was assumed to be understood by the fact that the mostly favored variant would form first, so the onset of the transformation, hence M_S was directly related with the maximum driving force available in the system. Application of this study to the phase transformation kinetics may not describe the physics ongoing accurately. The reason is that, when a certain load is applied to the system, different mechanical driving forces would get resolved on variants, and affect their volumetric fraction in the resultant microstructure accordingly. In this aspect, there is not a single mechanical driving force available in the system, but all forming variants have their own mechanical driving forces resolved on them. Thus, while comparing the isothermal kinetics, it is important to

distribute the resolved mechanical driving forces in the system depending on variants, instead of taking the maximum mechanical driving force available in the system in order to compare with the chemical driving forces.

An experimental study was also done in order to obtain the angle distributions of the bainitic sub-units with respect to the applied loading [46], where it was calculated that the mostly favored orientation where the bainitic subunits were expected to form has an angle of $\theta=42°$ with respect to the stress axis. The experiments revealed the fact that the variants having an angle of 40°-50° with respect to the load axis were the ones that form most frequently. Other variants were also observed to form, even though with smaller frequencies [46].

An earlier study by Rees and Shipway [16] proposed a two dimensional model in order to predict the effect of stress and strain simultaneously. The model used a variant based approach in order to determine the mechanical driving forces resolved on each variant and the resultant kinetics rate and transformation plasticity. Examining the results, even though a general pattern was catched, the correct prediction of the phase transformation kinetics accompanying the transformation couldn't be modeled accurately due to the simplifications in the kinetics model. The model is still quite important since it has an approach of modeling the simultaneous growth of each bainitic variant in a competitive way and implements the necessary modifications in the kinetics theory in order to apply the general transformation kinetics model to a variant based model. The study given in this thesis also depends on a variant based model. Even though the deformations generated with the transformation wasn't modeled as given by [16], but adopted another approach [48] and applied further modifications, the study given by Rees and Shipway [16] is still quite important since it gives a good implementation to the variant growth models.

A recent study proposed by Han and Suh [49] developed a model in order to model the transformation plasticity during the bainite transformation. An initial problem with

the study was that, while calculating the transformation strains with the bainitic transformation, the full strain field that occurred with the formation of bainite wasn't calculated, and a partial strain field was taken into account for simplicity, which physically described the phenomena incompletely. Since the shear components weren't taken into account during determining the transformation strain fields, the anisotropy of the macroscopic transformation strains due the imposed stresses was tried to be modeled with the Kurdjumov-Sachs orientation relationship between the parent and product phases, where the orientation relationship of the 24 variants of the product phase was related with the parent phase. In the study, the volumetric fraction of each bainitic variant at the end of the transformation under constant stress was calculated with a probability function, where, in order to obtain the volumetric fraction of each bainitic variant, the ratio of the nucleation rate of a certain variant was divided by the total nucleation rate of all variants, which was termed as its probability to form. This approach simplified the model, since the actual transformation kinetics and the resultant transformation strains weren't needed to model together with the probability function. However, a limitation with the application of this theory was that, the validity of the model was checked for small stress levels, where all variants were forming. It should be noted that at higher stress levels, it was experimentally proved that some variant can't form [50].The study didn't take into account this effect, and the application of limited number of variants to the model in case of high stress levels, but still below the yield point, wasn't addressed. The amount of interaction energies between the stress fields and the transformation strain fields was also studied by Lee et al. [51], where the probability of the formation of a variant with its mechanical energy was compared.

A recent study gave detailed information regarding the stress-affected bainitic transformation and the resultant transformation strains and texture, both in terms of theory and experimental observations [50]. An important outcome of this study was that, certain variants get deactivated with high external loadings, which was proved

experimentally with the SEM-EBSD observations. Then, the related transformation strain calculations of the specimen in general shall be conducted then including this phenomenon. It was seen with the calculations that the degree of the anisotropy in the transformation strains increased when less variants were active in the system. During the transformation strain calculations, the model was fit to the experimental data, and the resultant number of active variants was obtained to determine the experimental transformation strains. A simplification done in the model in terms of obtaining the transformation plasticity was that, the amount of active variants in the system was assumed to have equal volumetric fractions, which may cause certain shifts during the final transformation strain calculations.

Within the study, an attempt was made in order to obtain a relation between the ratio of the mechanical driving force introduced to the system and the related number of active variants. A linear relation was obtained depending on some experimental data, however the extent of the experiments were limited [50]. The study however is quite important since the number of active variants in the system and its relation to the transformation anisotropy is extensively studied.

Studies focusing on the diffusion controlled growth of bainite and the following kinetics also exist in the literature, however these studies aren't focused in the current thesis [52-54], since as mentioned previously, extensive experimental evidences confidently sign a displacive mechanism for the growth mechanism of bainite [3].

Following the literature, it may be concluded that the current thesis follows the path of the literature, and deals with the stress affected bainitic transformations, with a specific aim of developing a model to predict the transformation strains and kinetics simultaneously.

Chapter 3

THEORY

3.1) Crystallographic Texture in Displacive Transformations

The aim of this section is to introduce the theory in order to obtain the crystallographic texture and transformation strains upon a displacive transformation, which is the case for a bainitic transformation. Most of the theory developed in order to predict the transformation texture is on martensitic transformations, but also applicable to the bainitic transformations [55].

In order to define the deformation mechanism during the austenite – γ face centered cubic (FCC) - to martensite - α body centered cubic (BCC) or body centered tetragonal (BCT) – transformation, a homogenous deformation mechanism was initially introduced [55]. The mechanism explained is illustrated in Figure 4 below [55]. Accordingly, considering the existence of a BCT unit cell within two FCC unit cells, the related displacive martensitic transformation can be obtained by compressing the existing BCT cell along the z axis, and uniformly expanding on the x-y plane. This homogenous deformation is called as Bain strain, **B**, given by [55]

$$\mathbf{B} = \begin{bmatrix} \sqrt{2}\frac{a_\alpha}{a_\gamma} & 0 & 0 \\ 0 & \sqrt{2}\frac{a_\alpha}{a_\gamma} & 0 \\ 0 & 0 & \frac{a_\alpha}{a_\gamma} \end{bmatrix} \tag{15}$$

where a_α and a_γ are the lattice parameters of the martensitic and austenitic phases respectively.

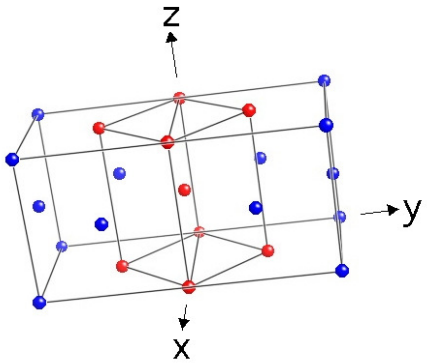

Figure 4: Two FCC and one BCT unit cell of austenite [55].

With the Bain strain, the following orientation relationship between the parent and product phase is obtained [55]

$$[0\ 0\ 1]_\gamma \parallel [0\ 0\ 1]_\alpha$$
$$[1\ \text{-}1\ 0]_\gamma \parallel [1\ 0\ 0]_\alpha$$
$$[1\ 1\ 0]_\gamma \parallel [0\ 1\ 0]_\alpha$$

A major problem with the definition of martensitic transformations with Bain strain is that, the proposed mechanism isn't possible for a displacive transformation. More specifically, a high level of continuity is needed across the interface plane of the austenitic and martensitic phases, with an invariant line existing on it [56]. This invariant line is defined as "joins the product and parent phases without any distortion and rotation" [56]. Existence of an invariant line on the interface plane would make the interface glissile with the movements of the dislocations across the interface, which produces the deformation and the change in crystal structure [56]. Figure 5 below illustrates the effect of Bain strain on the interface [55].

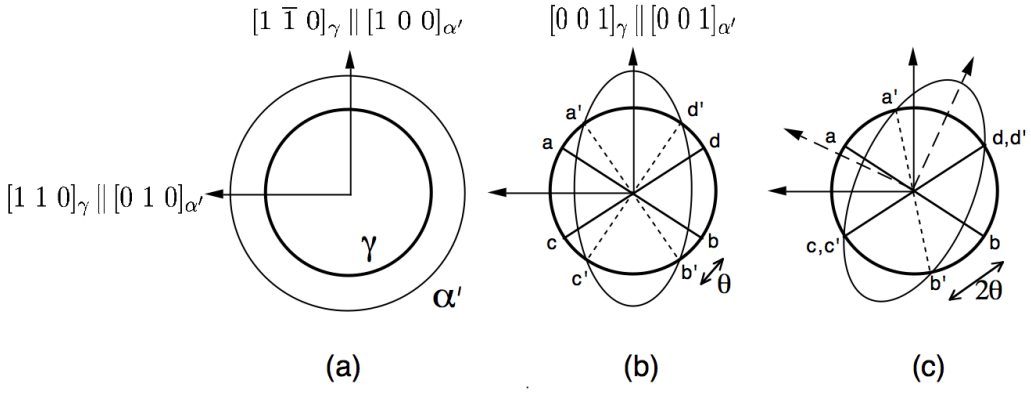

Figure 5: a) Austenitic phase b) The effect of Bain strain B c) Bain strain B and rotation R [55].

In Figure 5a, austenitic phase is represented as a sphere, which then forms an ellipsoid of revolution with the application of Bain strain [55]. It is seen clearly that all lines on the interface are either distorted or rotated. At this point, application of a further rotation to the system, **R**, produces an invariant line strain (ILS) as seen in Figure 5c with cd parallel to c'd', hence provides the semi-coherent interface for the displacive transformation [55]. Eventually, it is concluded that the Bain strain and a further rotation, **BR,** is needed to define the exact orientation relationship between the two phases [55].

A problem in understanding the nature of the transformation is that, even though the orientation relationship between the parent and product phases are determined with an ILS deformation, an invariant plane strain (IPS) deformation is observed in macroscale, with an undistorted and unrotated interface plane, which is called as habit plane [55]. This inconsistence with the proposed theory and the observed shape deformation is explained as follows. Examining Figure 6 below, which is for illustration [55], it is seen that the lattice deformation **BR** is an ILS, causing the deformation from (a) to (c) in the Figure [55]. On the other hand, the observed shape deformation is an IPS, $\mathbf{P_1}$, (a) to (b) with wrong crystal structure. With the application of a second homogenous shear $\mathbf{P_2}$, the correct crystal

structure is obtained with a wrong shape [55]. This may be explained with the phenomenological theory of martensite (Figure 6) [55,56]

$$\mathbf{P_1\ P_2 = BR} \tag{16}$$

which indicates a mathematical relationship between the orientation relationship between the product and parent phase and the shape deformation. The observed shape deformation with the correct crystal structure then can be obtained by introducing an inhomogeneous lattice-invariant deformation with twinning or slip, which would cancel the effect of $\mathbf{P_2}$ in macroscale [55].

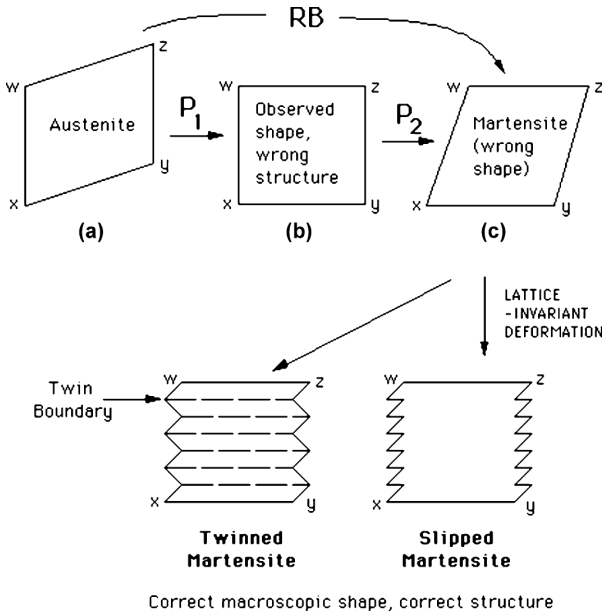

Figure 6: The phenomenological theory of martensite crystallography [55,56].

3.2) Transformation Strains and the Interaction Energy with the Applied Stress

In order to determine the interaction energy between the applied stress and the transformation strains, the macroscopic deformation should be taken into account [56].

Accordingly, it is the shape deformation $\mathbf{P_1}$ that should be used during the calculations [56]. The shape deformation accompanying the formation of z^{th} bainitic variant among the 24 variants with reference to the austenite coordinate frame is obtained with the formulation [56]

$$\mathbf{P}_{\gamma Z} = \mathbf{I} + m\, \mathbf{d}_\gamma\, \mathbf{p}_\gamma^{\mathbf{T}} \tag{17}$$

where $\mathbf{I}$ is the identity matrix, m is the magnitude of shape deformation, given by [57]

$$m = \left[s^2 + n^2\right]^{1/2} \tag{18}$$

where s is the shear and n is the dilatational strain on the habit plane. $\mathbf{p}_\gamma$ is the unit normal of the habit plane where transformation takes place, and $\mathbf{d}_\gamma$ is the displacement direction, which is also a unit vector. The superscript "T" denotes the matrix transpose. The magnitude of the shear and dilatation due to the transformation, the habit plane orientation and the displacement direction in the habit plane can be calculated by obtaining the lattice parameters of the parent and product phases [48]. Accordingly, the habit plane normal $\mathbf{p}_\gamma$ can be determined in terms of its direction cosines h, k, and *l* using the parameters η_1 and η_2, where [48]

$$\eta_1 = \frac{\sqrt{2}a_\alpha}{a_\gamma} \qquad \eta_2 = \frac{a_\alpha}{a_\gamma} \tag{19}$$

$$p_\gamma = \begin{bmatrix} h \\ k \\ l \end{bmatrix}$$

$$h = \frac{1}{2\eta_1}\left\{\sqrt{\frac{\eta_1^2 + \eta_2^2 - 2\eta_1^2\eta_2^2}{1-\eta_2^2}} - \sqrt{\frac{2-\eta_1^2-\eta_2^2}{1-\eta_2^2}}\right\} \tag{20}$$

$$k = \frac{1}{2\eta_1}\left\{\sqrt{\frac{\eta_1^2 + \eta_2^2 - 2\eta_1^2\eta_2^2}{1-\eta_2^2}} + \sqrt{\frac{2-\eta_1^2-\eta_2^2}{1-\eta_2^2}}\right\} \tag{21}$$

$$l = \frac{1}{\eta_1}\sqrt{\frac{\eta_1^2 - 1}{1 - \eta_2^2}} \tag{22}$$

$\mathbf{d}_\gamma$, the displacement direction in unit vectors with respect to austenite axis is determined with [48]

$$\mathbf{d}_\gamma = \frac{1}{N}\begin{Bmatrix} -[s - K(\lambda_1\lambda_2 - 1)]\cos\gamma \\ -[s - K(\lambda_1\lambda_2 - 1)]\sin\gamma \\ (\lambda_1\lambda_2 - 1) + sK \end{Bmatrix} \tag{23}$$

where

$$N^2 = \frac{(\lambda_1 - \lambda_2)^2(\lambda_1^2 - \lambda_2^2)}{\lambda_1^2 - 1} \tag{24}$$

$$K = \sqrt{\frac{1 - \lambda_2^2}{\lambda_1^2 - 1}} \tag{25}$$

$$\lambda_1 = \eta_1 \qquad \lambda_2 = \eta_1\eta_2$$

$$\cos\gamma = \sqrt{\frac{1}{2}(1 + \sqrt{1 - A^2})} \tag{26}$$

$$\sin\gamma = \sqrt{\frac{1}{2}(1 - \sqrt{1 - A^2})} \tag{27}$$

$$A = \frac{(\eta_1^2 - 1)(1 - \eta_2^2)}{1 - \eta_1^2\eta_2^2} \tag{28}$$

$$s = \sqrt{(\lambda_1^2 - 1)(1 - \lambda_2^2)} \tag{29}$$

Here s corresponds to the shear magnitude on the habit plane. The dilatation "n" in Equation (18) is given by [57]

$$n = \eta_1^2 \eta_2 - 1 \tag{30}$$

Figure 7 below illustrates the invariant plane strain with the shear and dilatation components [57].

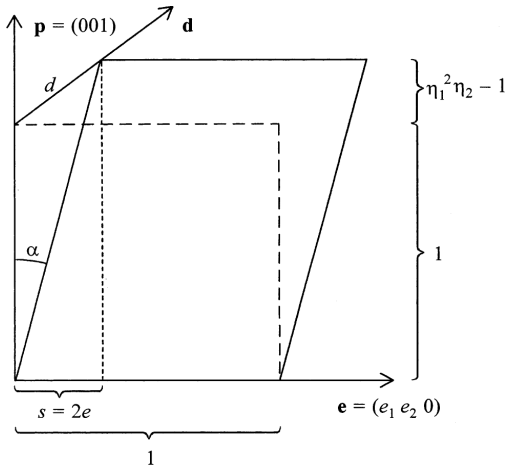

Figure 7: Invariant plane strain with simple shear s, uniaxial dilatation n, habit plane normal p, shape deformation direction d [57].

The lattice parameters at transformation temperature are determined to be $a_\gamma = 0.3605$ nm and $a_\alpha = 0.2884$ nm from density calculations of 51Crv4 steel using JMat Pro software for the material studied [1]. These lattice parameters correspond to a shear strain of s = 0.225 and a dilatational strain of n = 0.024 on the habit plane. The habit plane normal $\mathbf{p}_\gamma$ and the displacement direction $\mathbf{d}_\gamma$ for the calculated α – γ lattice parameters are determined as [48]

$$\mathbf{p}_\gamma = \begin{bmatrix} 0.5992 \\ 0.1825 \\ 0.7795 \end{bmatrix} \quad \mathbf{d}_\gamma = \begin{bmatrix} -0.6779 \\ -0.2065 \\ 0.7055 \end{bmatrix}$$

The deformation matrix given in Equation (17) is for a single variant, where the deformation matrices of the remaining 23 bainitic variants can be extracted from the

symmetry operations [58]. The deformation matrix of the z^{th} bainitic variant in the grain coordinate system $\mathbf{P}_{\gamma Z}$ can then be transformed into the specimen coordinate frame following [59]

$$\mathbf{P}_{SZ} = \mathbf{R}\,\mathbf{P}_{\gamma Z}\,\mathbf{R}^{T} \tag{31}$$

where $\mathbf{R}$ is the rotation matrix relating the grain coordinate frame to the specimen coordinate frame and $\mathbf{P}_{SZ}$ is the deformation matrix in the specimen coordinate frame. The rotation matrix is given by [50]

$$\mathbf{R} = \begin{bmatrix} \cos\phi_1 \cos\phi_2 - \sin\phi_1 \cos\phi \sin\phi_2 & \sin\phi_1 \cos\phi_2 + \cos\phi_1 \cos\phi \sin\phi_2 & \sin\phi \sin\phi_2 \\ -\cos\phi_1 \sin\phi_2 - \sin\phi_1 \cos\phi \cos\phi_2 & -\sin\phi_1 \sin\phi_2 + \cos\phi_1 \cos\phi \cos\phi_2 & \sin\phi \cos\phi_2 \\ \sin\phi_1 \sin\phi & -\cos\phi_1 \sin\phi & \cos\phi \end{bmatrix} \tag{32}$$

with ϕ_1 ϕ_2 and ϕ are the Euler angles, defining the rotation needed to make the local frame coincide with the reference frame [50].

Once the deformation matrix is obtained in the specimen coordinate frame, the transformation strain of z^{th} bainitic variant is given by [56]

$$\boldsymbol{\varepsilon}_{ij-z} = \frac{\mathbf{P}_{SZ} + \mathbf{P}_{SZ}^{T}}{2} - \mathbf{I} \tag{33}$$

and the interaction energy between the transformation strain of the bainitic variant and the applied stress with [56]

$$\mathbf{U}_z = \boldsymbol{\sigma}_{ij}\boldsymbol{\varepsilon}_{ij-z} \tag{34}$$

where $\boldsymbol{\sigma}_{ij}$ is the applied stress that is assumed to be equivalent to the internal stress field. The transformation strain tensor in Equation (33) refers to the complete bainitic transformation of a single variant, where for partial transformations the strain field is determined by [60]

$$\boldsymbol{\varepsilon}_{\mathbf{ij-z}} = \mathrm{f}\left(\frac{\mathbf{P}_{\mathbf{SZ}} + \mathbf{P}_{\mathbf{SZ}}^{\mathbf{T}}}{2} - \mathbf{I} \right) \tag{35}$$

with f defined as the volume fraction of the bainitic variant. Once the transformation strain field of each variant is calculated in the specimen coordinate frame, the total transformation strain of a single grain is obtained in the same coordinate frame with [49]

$$\boldsymbol{\varepsilon}_{\mathbf{ij}}^{\mathbf{TP}} = \sum_{z=1}^{N} \boldsymbol{\varepsilon}_{\mathbf{ij-z}} \tag{36}$$

Here, N is the number of the active bainitic variants forming in the grain, depending on the extent of applied stress and the resulting variant selection in the system [50]. It is important to mention that, when there is no applied load, there would be no favored variants, and all the variants would form in equal fractions. The stresses are limited to the yield strength of the material in the current work, since a stress-assisted transformation is considered. It should be noted that the transformation strains obtained up to this point from the solid-state phase transformation reflect the values for an ideal case, where there is no restriction in the deformation of the grain due to the solid-state phase transformation occurring inside. However, the deformation of a certain grain is restricted in the specimen due to the surrounding grains, and this effect could be incorporated with [61]

$$\boldsymbol{\varepsilon}_{\mathbf{ij}}^{\mathbf{G}} = \mathbf{S}_{\mathbf{ijkl}}\, \boldsymbol{\varepsilon}_{\mathbf{kl}}^{\mathbf{TP}} \tag{37}$$

where $\mathrm{S}_{\mathrm{ijkl}}$ is the Eshelby tensor. In this calculation, the geometry of a grain is assumed to be spherical, and the resulting tensor components are defined as [61]

$$S_{1111} = S_{2222} = S_{3333} = \frac{7 - 5\nu}{15(1 - \nu)} \tag{38}$$

$$S_{1122} = S_{2233} = S_{3311} = S_{1133} = S_{2211} = S_{3322} = \frac{5\nu - 1}{15(1 - \nu)} \tag{39}$$

$$S_{1122} = S_{2323} = S_{3131} = \frac{4 - 5\nu}{15(1 - \nu)} \tag{40}$$

with ν defined as the Poisson's ratio, taken as 0.3 for the current material.

The restriction on the deformation of a grain due to the surrounding bulk material can equivalently be applied to the deformation of a bainitic variant within an austenitic media in a grain, however; there is a distinction between the two cases. The approximation of the bulk material as an elastic medium may be a reasonable, however; during the formation of a bainitic variant, the growth of a single bainitic sub-unit ceases due to slip in the system and the resulting resistance against further lattice deformation [39, 43]. At this point, it is difficult to obtain the extent of deformation accommodated in the matrix due to the significant amount of plastic deformation in the parent matrix. Consequently, this effect was not taken into account in the sub-unit scale in the current model for the sake of simplicity. Accordingly, for a total number of I grains, the resulting transformation strain tensor on the macroscale can be defined as

$$\boldsymbol{\varepsilon}_{\mathbf{ij}}^{\mathbf{TR}} = \frac{1}{\mathrm{N}} \sum_{\mathrm{m=1}}^{\mathrm{I}} \boldsymbol{\varepsilon}_{\mathbf{ij}}^{\mathbf{G}} \tag{41}$$

with the assumption that all grains satisfy the iso-stress condition and have the same volume [49]. The simulations are carried out on a 100 grain aggregate, where the orientations of grains are provided by experimental electron backscatter diffraction (EBSD) data.

3.3) Transformation Kinetics

The transformation kinetics calculations is adopted from Matsuda and Bhadeshia [15], with modifications in order to apply the general transformation model to variant-based simulations

The bainitic transformation kinetics of a single variant is characterized by the nucleation function [15]

$$I_z = \frac{K_1 \nu}{N} \exp\left[-\frac{K_2}{RT}\left(1 + \frac{\Delta F_m - \gamma U_z}{K_3}\right)\right] \quad (42)$$

where I_z is the nucleation rate of the z^{th} bainitic variant, ΔF_m is the maximum free energy available for a para-equilibrium nucleation, and is equated to $\Delta G^{\gamma \rightarrow \gamma' + \alpha}$, the chemical free energy change for the paraequilibrium transformation of austenite into ferrite and carbon-enriched austenite for simplicity [38]. The term γ stands for the molar volume, U_z is the mechanical driving force (MDF) resolved on the z^{th} variant, R is the universal gas constant, T is the absolute temperature, and ν is the attempt frequency factor, given as

$$\nu = \frac{k_B T}{h} \quad (43)$$

with k_B is the Boltzmann and h is the Planck constant. K_1, K_2 and K_3 are the fitting parameters, where K_3 was determined to be 2540 J mol^{-1} [15] and the remaining two are determined by fitting the simulation to the experimentally determined isothermal transformation curve. K_1 physically represents the effect of initial nucleation site density, and since each bainitic variant is modeled, following the approach introduced by Rees and Shipway [16], the number of total nucleation sites is divided by the term N in Equation (42), which corresponds to the number of active variants in the system. The original study isn't based on variants, but defined the general isothermal transformation kinetics [15]. At this point, the statement of the current thesis is that, in order to determine the transformation kinetics and transformation strains simultaneously, a variant based model shall be applied, in order to distribute the MDF correctly to the variants, hence obtain the resultant transformation anisotropy, due to varying bainitic variant fractions.

For zero applied stress, N is 24, where all variants are active. Considering the driving force calculations governing the transformation kinetics of the system, after removing the 400 J/mol of elastic strain energy stored in a bainitic variant, the chemical

free energy change of the current system was calculated to be 950 J/mol for an FCC γ to BCC α transformation [45,46]. It is also confirmed that the free energy available at the transformation temperature, 340 °C, satisfies both the nucleation at growth criteria mentioned previously.

During the transformation, the partition of carbon from bainite to austenite makes the parent phase more stable as the transformation proceeds [8]; however, an important point to mention about the transformation kinetics is that, the current material is considered to undergo complete phase transformation. It was experimentally observed that the excessive carbon diffusing from the product phase into the parent phase after the displacive transformation caused cementite precipitation in the residual matrix, instead of diffusing into parent austenite and stabilizing it [14]. This is due to the low silicon (Si) content in the material. Accordingly, stabilizing effect of carbon was not included in the current calculations.

For the sake of simplicity, cementite precipitation was not taken into account in the current work, since it had earlier been shown that the bainitic ferrite fraction is over 90% of the product phase [3,62,63]. The original kinetics model had been applied to steels with high-Si concentrations [15], where bainitic ferrite and the austenite were the two existing phases. The excessive carbon concentration in the product phase diffused into the residual austenite matrix and stabilized it, since the high-Si content suppressed the formation of cementite.

The additional factors introduced to the bainitic variant growth model by Rees and Shipway [16], which took into account the autocatalysis process and rate of decrease in the growth rate as transformation gets closer to saturation, is not considered in the current work. Instead, a recent model is used for the calculations, where the bainitic fraction is modeled in an incremental fashion, by taking into account the change in the volume fraction of bainitic sheaves at each time increment of the transformation [15].

The kinetics of phase transformation is based on the extended volume to extended area approach, where a space is assumed at which the product phase can nucleate at the already transformed regions and can grow within each other [15,64-66]. Considering a planar grain boundary and a parallel test plane with a "y" distance away from boundary, the increment in the extended area occurring with the intersection of the formed z^{th} bainitic variant and the test plane then may be defined as $\Delta O^{e}_{\beta,z,y}$ [15].

In order to obtain the real extend of transformation, a correction of this assumption is made by using a simple probability function. Accordingly, the relationship between the real and extended area of bainitic variant intersected with a test plane is given by [15]

$$\Delta O_{\beta,z,y} = \left(1 - \frac{O_{\beta,z,y}}{O_B}\right)\Delta O^{e}_{\beta,z,y} \tag{44}$$

with O_B is the total area of the grain boundary and $O_{\beta,z,y}$ is the real area at the intersection plane [15]. The increment of the extended area is calculated with [15]

$$\Delta O^{e}_{\beta,z,y} = \sum_{k=0}^{m} E_{k,m,y} O_B I_z \Delta t \tag{45}$$

In Equation (45), $E_{k,m,y}$ represents the change in the intersection area at the test plane during the time interval $m\Delta t$ to $(m+1)\Delta t$, due to the nucleations between the time $k\Delta t$ and $(k+1)\Delta t$ [15]. The term I_z is the nucleation rate of the z^{th} bainitic variant per unit area, and the term $O_B I_z \Delta t$ defines the number of extended particles nucleated in the given time interval [15]. Accordingly, the increment in the real area of the bainitic variant at "y" distance from the grain boundary at the given time interval is given by [15]

$$O_{\beta,z,y,t+\Delta t} = O_{\beta,z,y,t} + \Delta O_{\beta,z,y} \tag{46}$$

The extended volumetric increment of the variant is obtained by integrating the increment of the real area across the grain with [15]

$$\Delta V^{e}_{\beta,z} = \Delta y \sum_{y=0}^{q\,max} \Delta O_{\beta,z,y} \tag{47}$$

where Δy is a small distance within y, and q^{max} is the maximum length of the bainite sheaves [15]. The change in the real volume of the bainitic variant can be expressed in terms of a probability function as previously done in determining the real change in the intersected area at the test plane [15]

$$\Delta V_{\beta,z} = \left(1 - \frac{V_{\beta,z}}{V_T}\right) \Delta V^{e}_{\beta,z} \tag{48}$$

The resulting increment in the volumetric fraction of bainitic variant within the time interval Δt is then given by [15]

$$V_{\beta,z,t+\Delta t} = V_{\beta,z,t} + \Delta V_{\beta,z} \tag{49}$$

Accordingly, the evolution of the sheaf length through the transformation is given with [15]

$$\Delta q_k = \begin{matrix} 0 & \left[(m+1)\Delta t - n_k \Delta t < \Delta t_z\right] \\ l_u & \left[(m+1)\Delta t - n_k \Delta t \geq \Delta t_z\right] \end{matrix} \tag{50}$$

where Δq_k is the increment in the length of a bainitic sheaf, l_u is the length of a sub-unit, taken as 10 microns. The difference term in the Equation (50) correspond to the time interval between the current time $(m+1)\Delta t$ and the time at which the last nucleation had occurred, $n_k \Delta t$. If this interval is assumed to be higher than Δt_z, the time needed to have a nucleation of a new bainitic sub-unit at the tip of the existing sub-units, then it is assumed that the sheaf length is increased with the formation of the new bainitic sub-unit. Δt_z is obtained with [15]

$$\Delta t_z = \frac{1}{I_z} \tag{51}$$

Upon the nucleation of the new bainitic subunit, $n_k \Delta t$ is equated to $(m+1)\Delta t$ [15]. The change in the sheaf length is updated with [15]

$$q_{k(m+1)\Delta t} = q_{k,m\Delta t} + \Delta q_k \tag{52}$$

The thickening of sheaves with the nucleation of sub-units cause a change in the intersection area at the test plane, and this is taken into account with [15]

$$E_{k,m,y} = \begin{cases} S_U & [n_k \Delta t = (k+1)\Delta t] \\ 0 \quad \text{if} & [(m+1)\Delta t - n_k \Delta t < \Delta t_z] \\ \theta S_U & [(m+1)\Delta t - n_k \Delta t \geq \Delta t_z] \end{cases} \tag{53}$$

where the autocatalysis factor θ is taken as 2, and S_U is the surface area of the bainitic sub-unit per unit volume [15].

In order to adopt the general kinetics model for variant based calculations, the time tracker $n_k \Delta t$ is applied independently for each 24 variants in an austenite grain in stress free calculations, or in other words, the above proposed model is applied for each bainitic variant. It is important to mention that the number active of variants to be modeled may change, depending on the applied stress level.

The increase in the volumetric fraction of each bainitic variant is then calculated independently from each other, by calculating the nucleation rates in accordance with the resolved mechanical driving forces and the related time needed for the successive formation of the next bainitic sub-units Δt_z. During the calculations, while applying the probability function in order to estimate the correct fraction of the formed phase bainitic variant, sum of all variants are taken into account, which relates the output of all variants with each other. Accordingly, Equation (44) and (48) are modified as [67]

$$\Delta O_{\beta,z,y} = \left(1 - \frac{\sum_{i=1}^{N} O_{\beta,i,y}}{O_B} \right) \Delta O^e_{\beta,z,y} \tag{54}$$

$$\Delta V_{\beta,z} = \left(1 - \frac{\sum_{i=1}^{N} V_{\beta,i}}{V_T} \right) \Delta V_{\beta,z}^{e} \tag{55}$$

where N is the number of active variants in the system.

The original usage of the kinetics model was for a stress free transformation [15]. In other words, the growth of a sheaf was modeled, which consists of bainitic sub-units with identical orientations. In this aspect, the original model can be applied to a stress-free transformation since all sheaves with different orientations have equal probability to form with equal nucleation rate, and it is enough to model a single sheaf in terms of kinetics. The resultant transformation strain field will of course need extra considerations, by taking into account the growth of all sheaves [15].

In the current study, the kinetics model described above is applied to each variant independently, since each variant has a different nucleation rate and Δt_z due to the applied external stress. With this modification, it is possible to obtain the volumetric fraction of each variant through the transformation, where the original model gives the total volumetric fraction of the product phase as an output [15].

Chapter 4

EXPERIMENTAL PROCEDURE

The material investigated in this study is a low-alloy 51CrV4 steel with a chemical composition tabulated in Table 1. Precisely machined thin-walled hollow specimens with an outer diameter of 10 mm were used in the experiments, with a wall thickness of only 1 mm within the gage length. The specimens were austenitization at 1200 °C for 10 seconds (heated up within 15 seconds), and then quenched with pressurized gas down to a temperature of 340 °C at a nominal cooling rate of 45°C/s. The isothermal transformation data is recorded for zero stress and true tensile stresses of 50 MPa and 140 MPa.

Table 1: Chemical composition of the material studied. The data was shown to represent minimum and maximum values obtained from various samples.

Element	**C**	**Cr**	**Mn**	**S**	**Pb**	**Si**	**Cu**
Mass contents in %	0.48 0.48	0.88 0.94	0.72 0.77	0.018 0.021	0.004 0.010	0.26 0.30	0.17 0.19
Element	**Al**	**Ni**	**Mo**	**Nb**	**Ti**	**P**	**Fe**
Mass contents in %	0.007 0.009	0.09 0.10	0.02 0.02	0.001 0.002	0.011 0.014	0.017 0.021	Balance Balance

In Figure 8 and 9, the specimen is in austenization treatment, before the quenching process. Figure 10 is an illustration of the experimental setup, where the 51CrV4 specimen is placed in a loading setup and surrounded by thermal load devices.

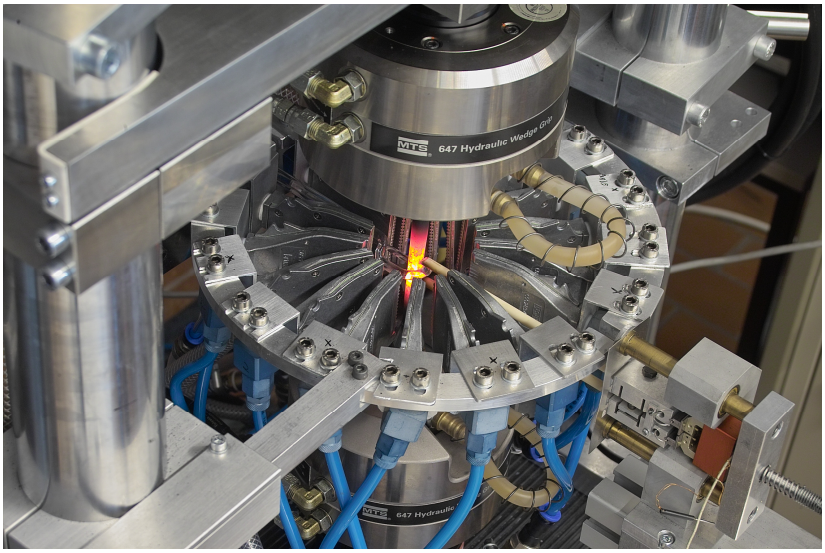

Figure 8: Specimen during the austenitization process at 1200 °C

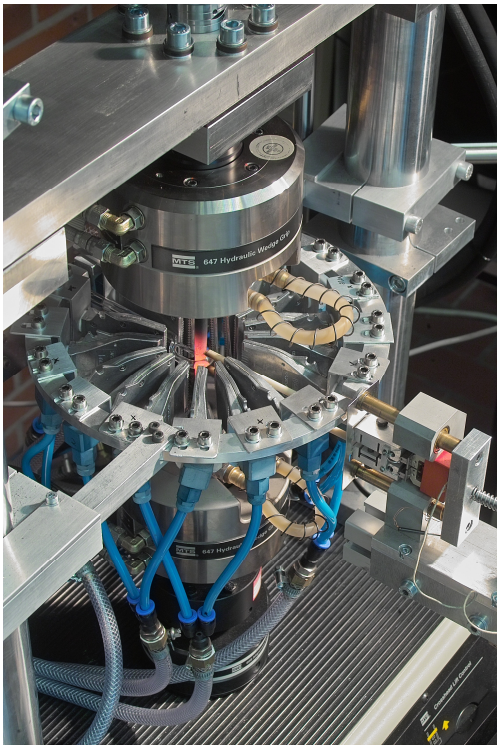

Figure 9: Specimen during the heating process to 1200 °C

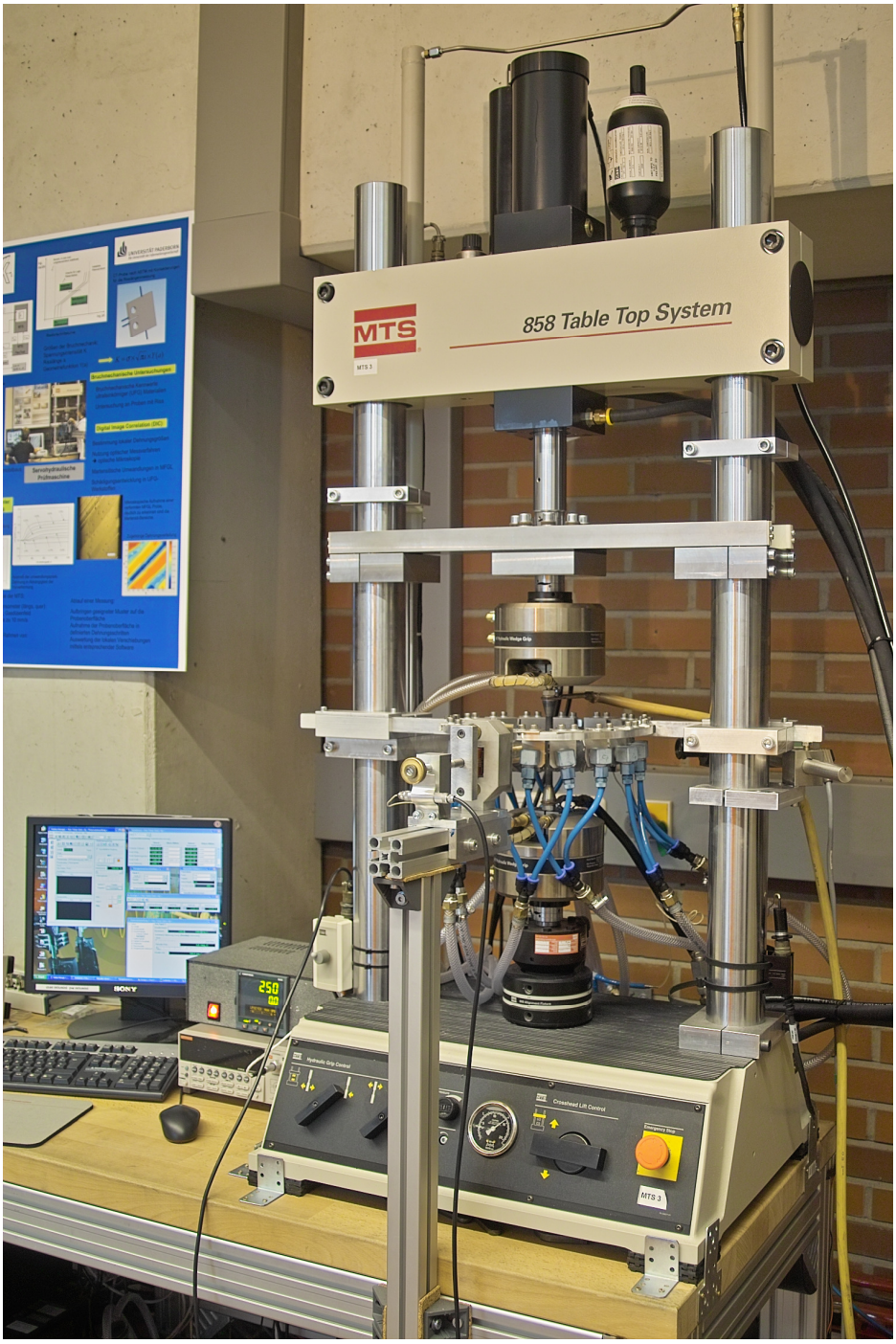

Figure 10: Thermomechanical treatment setup.

Chapter 5

RESULTS AND DISCUSSION

The austenite-to-bainite phase transition is accompanied by a volume change [14]. The change in the volume of a specimen undergoing bainitic transformation is determined from the simultaneously measured axial ε_a and diametral strains ε_d with the formulation [14]

$$\frac{\Delta V}{V} = (1+\varepsilon_a)(1+\varepsilon_d)^2 - 1 \tag{56}$$

where, the bainitic volume fraction f(t) at a certain time through the transformation is given by [14]

$$f(t) = \frac{\frac{\Delta V}{V}(t)}{\frac{\Delta V}{V}(t \to \infty)} \tag{57}$$

$\frac{\Delta V}{V}(t \to \infty)$ corresponds to the volume change in the time interval at which transformation gets saturated. In the current case, it is assumed that f =1 at the end of the transformation, which means that the material transforms to the product phase completely.

Experimentally determined isothermal transformation curves are presented in Figure 11 for the 51CrV4 sample under constant stresses of 50 MPa and 140 MPa, and in stress-free condition. Accordingly, under 50 MPa constant tensile stress the increase in the rate of transformation is not significant as compared with the stress-free transformation. Under 140 MPa constant stress, which is still below the yield strength, a significant increase in the rate of the transformation is notable. This can be attributed to the large mechanical driving forces resolved on the bainitic variants, whose magnitudes are

comparable to that of the chemical driving force available in the system, and thus, influence the transformation kinetics.

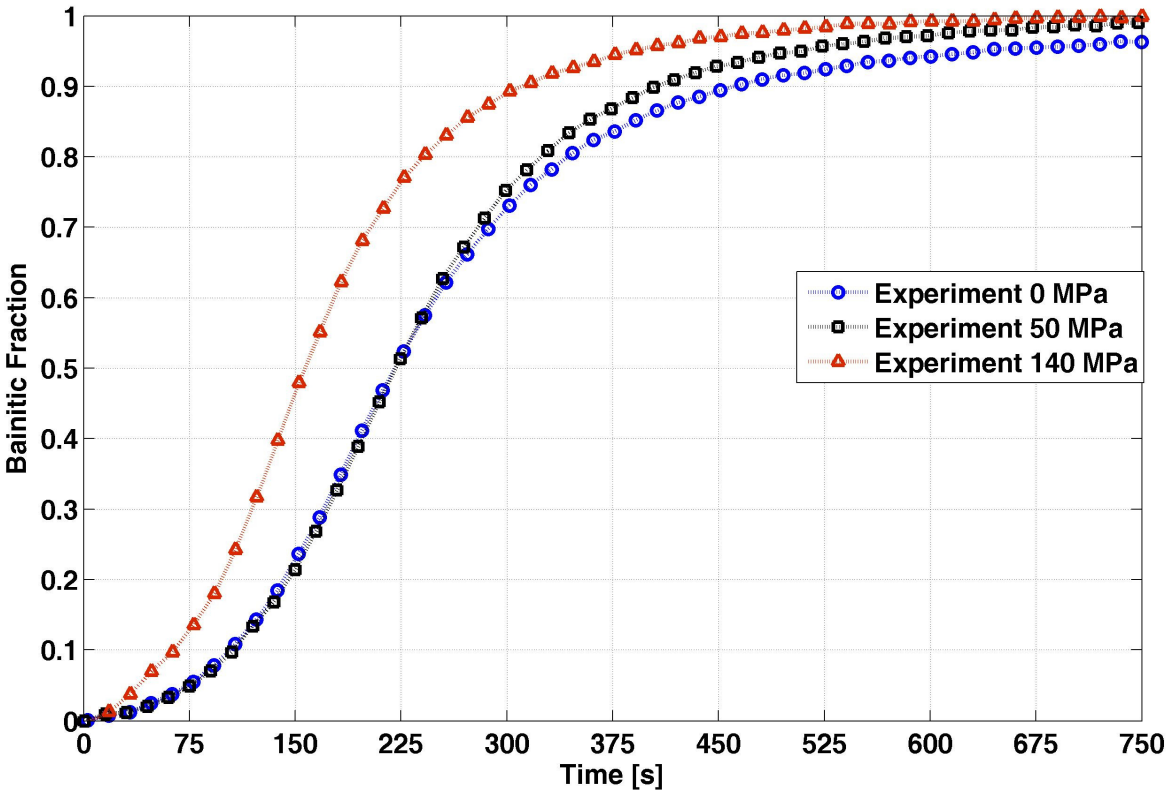

Figure 11: Isothermal transformation curves under constant tensile stresses.

The aim of the original model is to calculate the sheaf growth during the bainitic transformation. The model doesn't calculate the incubation period, where the nucleation takes place. Formation of small nuclei isn't detectable in macroscale in this period and the volume fraction of the product phase in the isothermal transformation curve stays at zero until the growth process starts. In Figure 11 above and following figures below, the incubation period isn't given, since it is out of scope of the study. From the first second, it is seen that the bainitic fraction is increasing, since the growth process is of interest.

In the current simulations, first the fitting parameters in Equation (42) were determined by fitting the simulation to the experimental data obtained under stress-free condition, and a good agreement was obtained between the experimental and simulation results (Figure 12). Since there is no applied loading on the system, the nucleation rate of each bainitic variant should be equal to each other for the stress-free isothermal transformation case, hence equal fractions of 24 bainitic variants are expected to form. The computational result yielded an equal volumetric fraction of 4.16% for each bainitic variant at 750 second, which is also in good agreement with the experimental data. The model outcome for Grain #1 can be found in Table 2 for illustration.

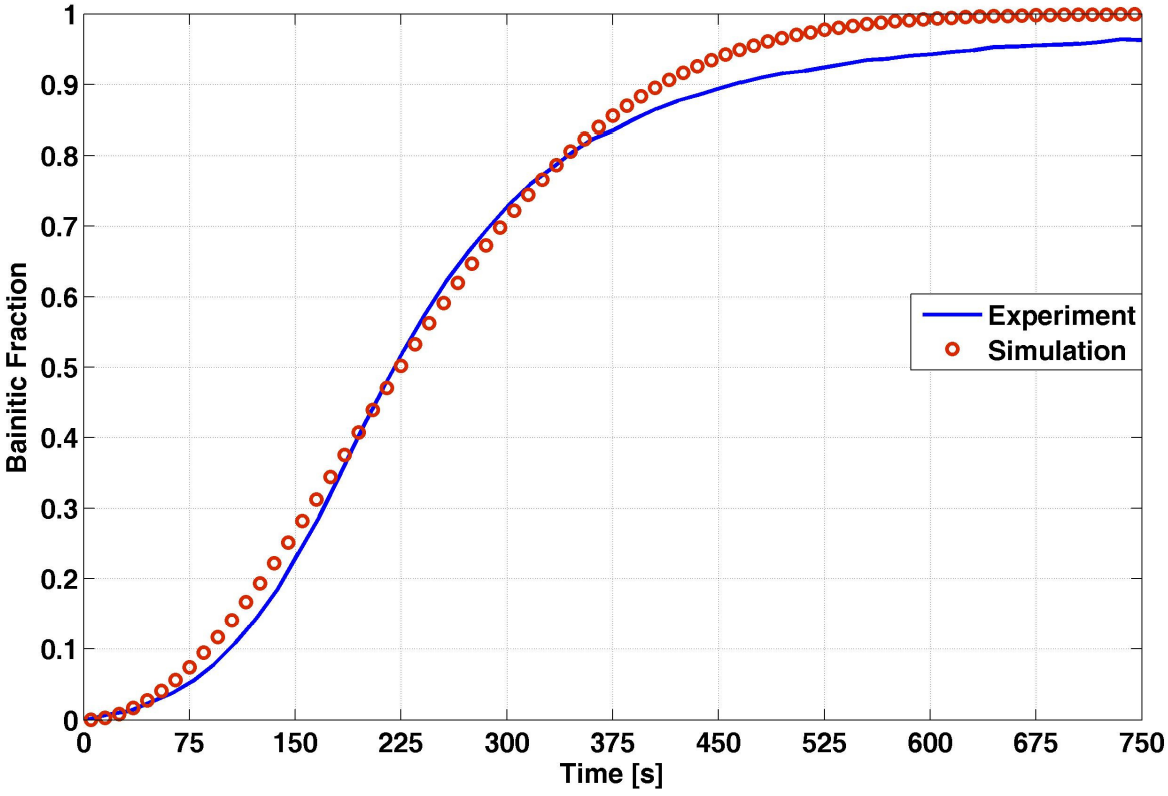

Figure 12: Comparison of simulation and experiment results for stress-free isothermal transformation.

Table 2. Resolved driving forces and the volumetric fractions of each bainitic variant in Grain #1 for zero stress.

Variant No.	Resolved Mechanical Driving Force	Volumetric Fraction	Variant No.	Resolved Mechanical Driving Force	Volumetric Fraction
1	0	0.0416	**13**	0	0.0416
2	0	0.0416	**14**	0	0.0416
3	0	0.0416	**15**	0	0.0416
4	0	0.0416	**16**	0	0.0416
5	0	0.0416	**17**	0	0.0416
6	0	0.0416	**18**	0	0.0416
7	0	0.0416	**19**	0	0.0416
8	0	0.0416	**20**	0	0.0416
9	0	0.0416	**21**	0	0.0416
10	0	0.0416	**22**	0	0.0416
11	0	0.0416	**23**	0	0.0416
12	0	0.0416	**24**	0	0.0416

The extent of the variant selection was computed and compared with the available data in the literature for the applied stresses of 50 MPa and 140 MPa [50]. As seen in Figure 13, the higher the ratio between the average of maximum MDF of 100 grains and the total driving force (TDF) of the system, the higher the extent of the variant selection with less number of active variants. (Getting the maximum MDF of all grains in the system and comparing it with the TDF during the active variant determination process is a method proposed by Kundu, Kase and Bhadeshia [50].) This also means more anisotropy in transformation strains at the macroscale. Previously, axial transformation strain of a polycrystalline material had been computed under a constant stress of 200 MPa, such that a 1% transformation strain due to 23 active variants became 5% with 4 active variants [50]. Once the MDF and TDF were obtained for the current system for the applied stresses of 50 MPa and 140 MPa, the corresponding active variants were determined by fitting the simulation to the experimental results [50]. Computed MDF is tabulated in Table 3 for the

two loads applied. The computed number of active variants stands in good agreement with the literature (Figure 13).

Table 3. Average of the maximum MDF resolved on 100 grains and its ratio to TDF.

Applied Stress [MPa]	**ΔG_{MECH} [J/mol]**	**ΔG_{CHEM} [J/mol]**	**$\Delta G_{MECH} / \Delta G_{TOTAL}$**
50	31	950	0.032
140	88	950	0.085

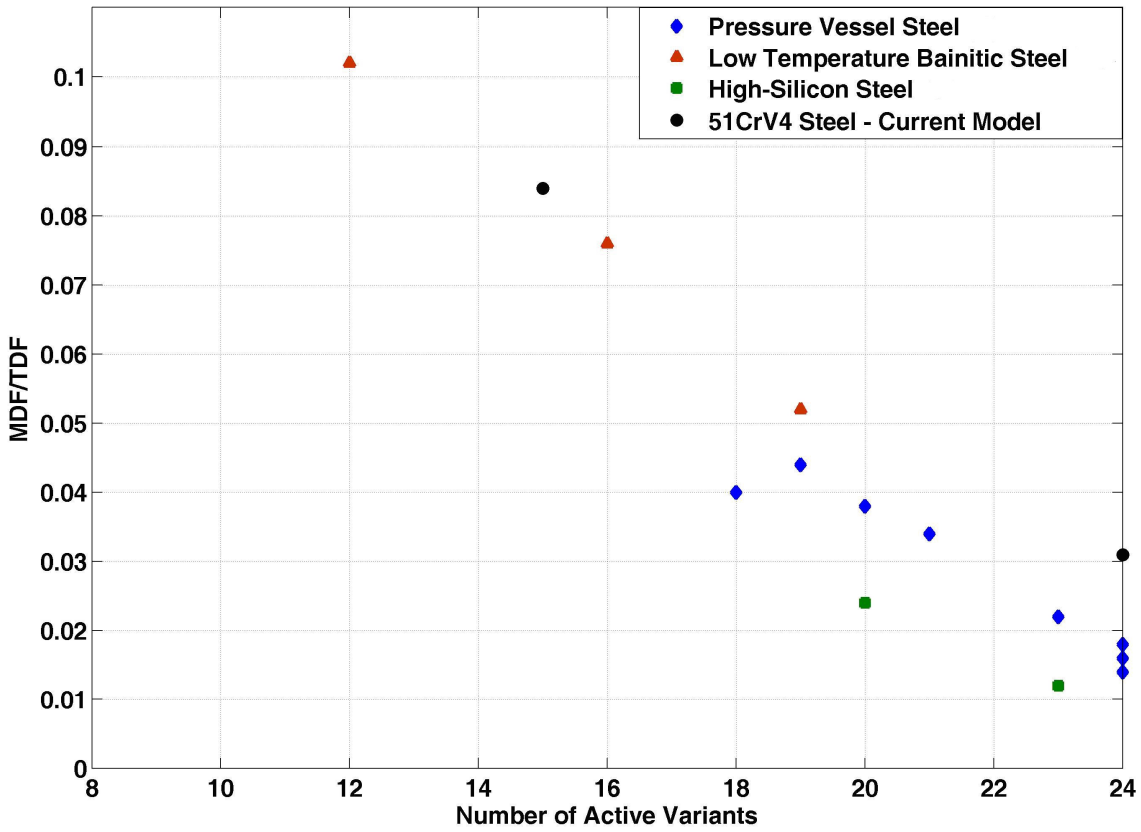

Figure 13: Relation between magnitude of the mechanical driving force introduced to the system and the resultant number of active variants [50].

As for the 50 MPa and 140 MPa constant stress cases, the experimentally observed behavior was closely predicted by the current model (Figure 14). Consequently, the experimentally observed increase in the rate of transformation as the applied stress was increased from 50 to 140 MPa was also captured by the current model. Specifically, 15 variants were predicted to be active in the case of 140 MPa applied stress by the model, due to higher MDF introduced to the system, whereas all 24 variants were favored in the stress-free transformation. The model output of the variant selectivity and the resulting volumetric fractions of the active variants for Grain #1 for the 50 MPa and 140 MPa applied stress

levels are presented in Tables 4 and 5, respectively, in the same fashion as provided for the stress-free case in Table 2. A similar transformation pattern was determined for a similar alloy composition and temperature range in a previous study [46], where a decrease in temperature, i.e., an increase in chemical free energy available in the system, reduced the effect of the applied stress on the transformation kinetics.

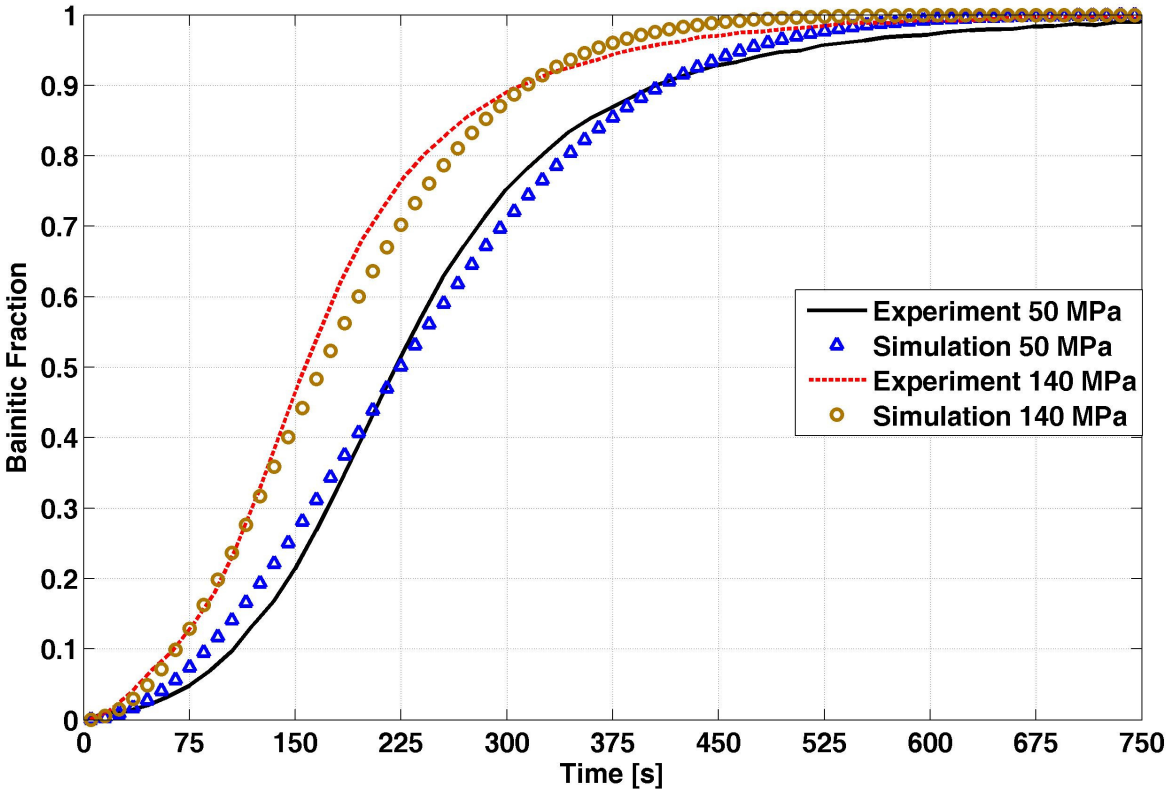

Figure 14: Comparison of simulation and experiment result for 50 MPa and 140 MPa applied stresses.

Table 4. Resolved driving forces and the volumetric fractions of each bainitic variant in Grain #1 for 50 MPa applied stress.

Variant No.	Resolved MDF [J/mol]	Volumetric Fraction	Variant No.	Resolved MDF [J/mol]	Volumetric Fraction
8	27.0	0.0602	**3**	1.5	0.0426
7	24.6	0.0596	**1**	0.3	0.0424
14	23.7	0.0594	**22**	-1.1	0.0421
2	22.0	0.0466	**17**	-5.7	0.0334
15	18.2	0.0458	**11**	-5.8	0.0334
13	18.1	0.0458	**10**	-9.2	0.0329
9	15.5	0.0453	**18**	-9.3	0.0329
23	12.3	0.0446	**5**	-11.8	0.0325
21	11.4	0.0445	**6**	-16.2	0.0319
16	9.8	0.0441	**12**	-17.1	0.0318
24	4.0	0.0430	**19**	-21.1	0.0313
4	3.1	0.0429	**20**	-26.4	0.0305

Table 5. Resolved driving forces and the volumetric fractions of each bainitic variant in Grain#1 for 140 MPa applied stress.

Variant No.	Resolved MDF [J/mol]	Volumetric Fraction	Variant No.	Resolved MDF [J/mol]	Volumetric Fraction
8	75.4	0.0997	**3**	4.1	0.0442
7	69.0	0.0969	**1**	0.8	0.0435
14	66.5	0.0959	**22**	-3.1	0.0428
2	61.7	0.0939	**17**	-16.1	Inactive
15	50.8	0.0686	**11**	-16.2	Inactive
13	50.6	0.0685	**10**	-25.8	Inactive
9	43.4	0.0664	**18**	-26.0	Inactive
23	34.5	0.0638	**5**	-33.1	Inactive
21	32.1	0.0632	**6**	-45.3	Inactive
16	27.4	0.0619	**12**	-47.8	Inactive
24	11.3	0.0456	**19**	-59.1	Inactive
4	8.7	0.0451	**20**	-74.0	Inactive

The simulation results indicate that the volumetric fractions of the bainitic variants are not equal anymore at the end of the transformation in the cases of applied non-zero

stresses (Tables 2, 4 and 5). However, the bainitic volume fractions depend on the MDF resolved on the variant due to the applied external stress, where the most favored variant has the highest volumetric fraction (Tables 4 and 5). For instance, as the applied stress is increased from 50 MPa to 140 MPa, 15 variants form, where the volumetric fractions of the active variants are dependent on the resolved MDF and the unfavored 9 variants are inactive. This is due to the high ratio between the MDF and TDF, which means that, as the applied load increases, the corresponding transformation anisotropy will also increase due to the reduced number active variants. Figures 15 and 16 give the MDF resolved on each variant for two grain orientations, labeled as "Grain A" and "Grain B", for illustration.

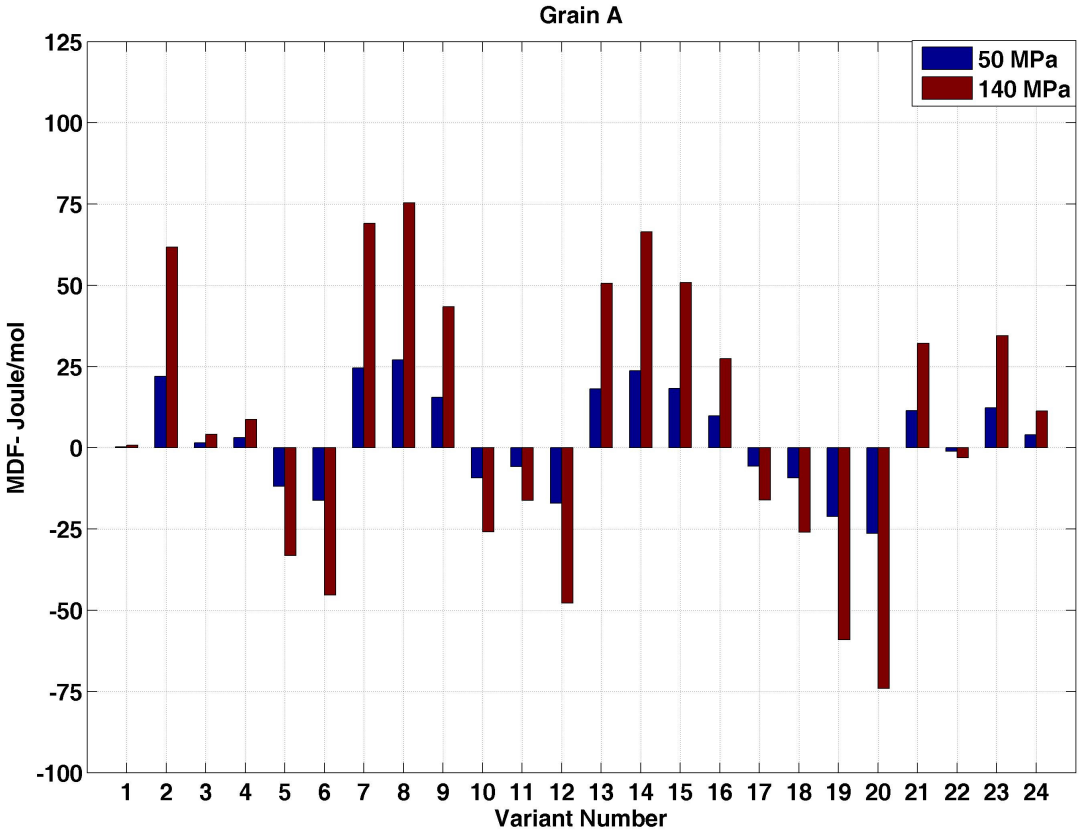

Figure 15: MDF resolved on bainitic variants for Grain A.

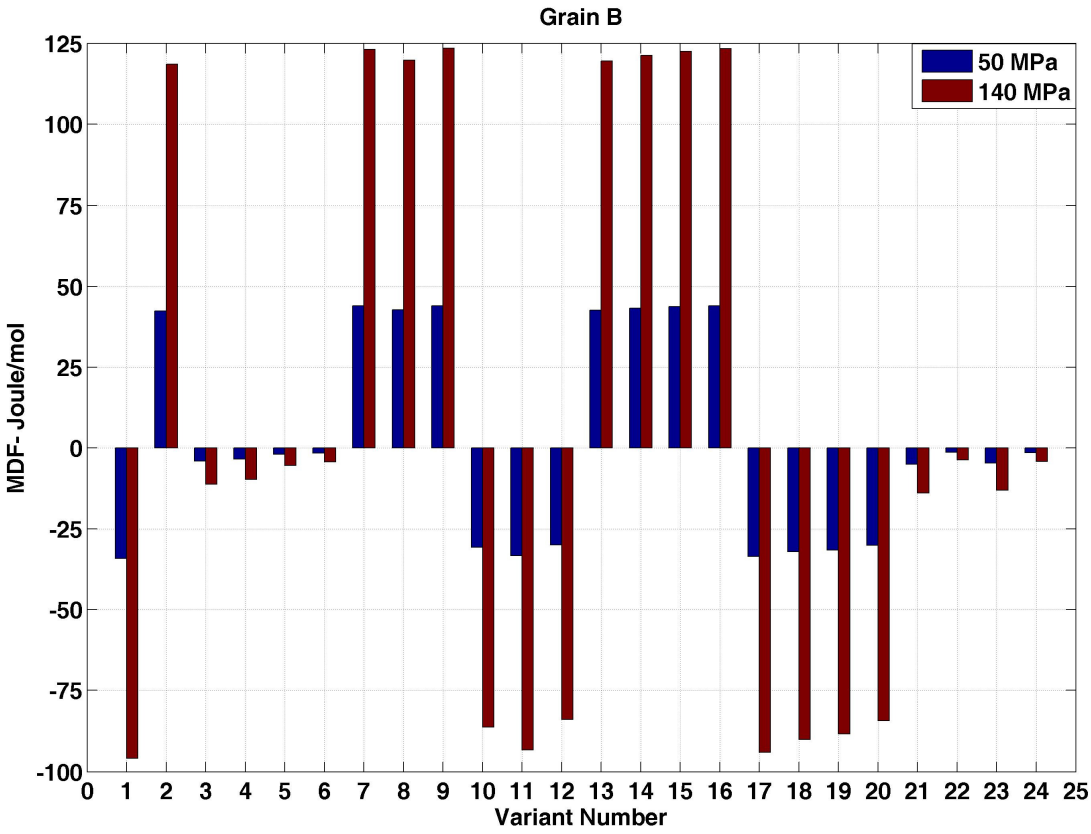

Figure 16: MDF resolved on bainitic variants for Grain B.

Figures 17 and 18 present the measured axial and radial strains and in comparison with computed values during stress-free transformation and transformation under constant applied stresses. The experimental measurements revealed that, as the applied stress increases, the related transformation anisotropy increases, as well. The higher values of strain is associated with the extent of variant selection in the system, such that, as the number of favored variants decreases with the increase in the applied stress, the magnitude of the macroscopic transformation strain also increases due to the increasing anisotropy at the microscale [50]. In the stress-free condition, it is clearly seen that the magnitude of the

axial and radial strains are almost equal to each other, which stems from the fact that all variants are active and equivalently favored, leading to an isotropic transformation strain in the macroscale. The computed strain values utilizing the current model stand in very good agreement with the experimental data (Table 6).

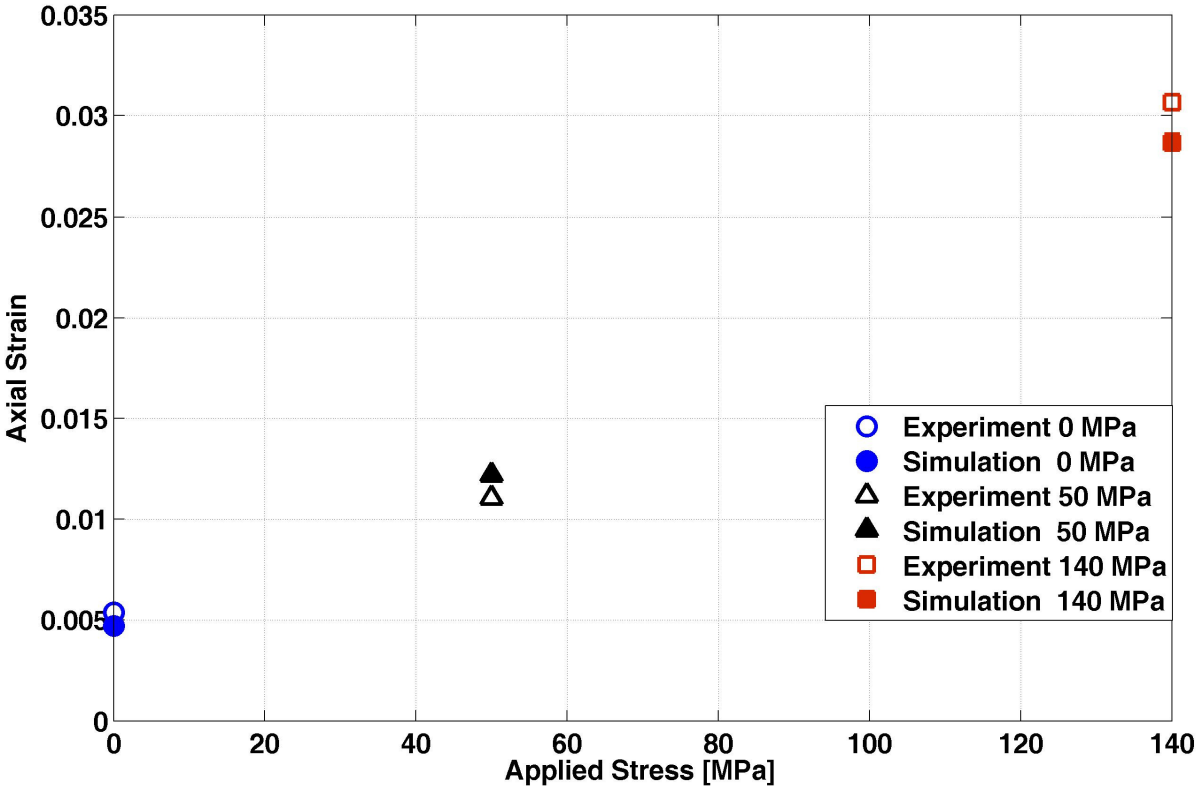

Figure 17: A comparison of axial transformation strain data obtained from experiments and simulations.

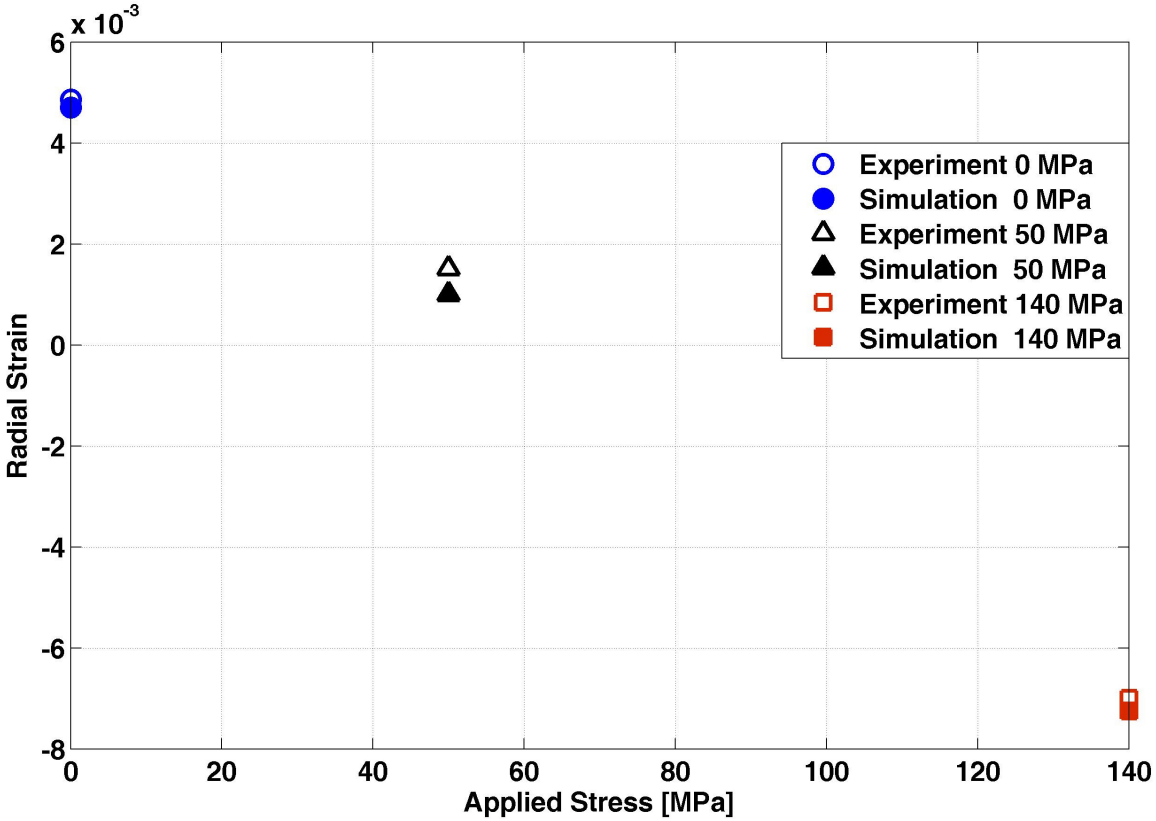

Figure 18: A comparison of radial transformation strain data obtained from experiments and simulations.

Table 6. Comparison of experiment and simulation results of axial and radial strains under stress-free and constant stress conditions.

Applied Stress [MPa]	Axial Strain Experiment	Axial Strain Simulation	Radial Strain Experiment	Radial Strain Simulation
0	0.0054	0.0047	0.0049	0.0047
50	0.0110	0.0122	0.0015	0.0010
140	0.0306	0.0287	-0.0070	-0.0072

Even though there are experimental studies on the number of active variants under various stress levels [50], a general mathematical relationship between the MDF–to–TDF ratio and the number of active variants available in a system has not been forwarded yet. For establishing such a relationship, extensive experimental studies monitoring the number of active variants in a system under various stress levels should be systematically carried. However, such data is not available in the literature yet. Thus, instead of determining the number of active variants in a system under constant external stress directly from the MDF-TDF relationship, a fitting procedure was employed to determine the number of active variants, since transformation strain is directly associated with the number of variants active in the system.

Previously, the experimental radial strain values were utilized during the fitting process to determine the number of active variants accordingly, and only a comparison with the computed and measured radial strains were given with a reasonable number of active variants in the system [50]. The current model utilizes the axial transformation strains for the initial fitting to calculate the extent of the active variants, where it is also seen that with the resultant variant choices, the computed radial strains and transformation curves are also in good agreement with the experimental data, which confirm the success of the current model.

The application of the variant-based kinetics model to compute the isothermal transformation behavior and the resultant transformation strains yielded close prediction of the experimental data. The current results show that the proposed model is capable of computing the volumetric fraction of each active variant, the resultant transformation strains and the corresponding isothermal kinetics curve. The extent of the variant selectivity and the number of active variants computed stand in good agreement with the literature, as well. Still, a difference exists between the experimental and computed axial and radial strains, which may be due to several reasons.

One possible reason may be the way the variant formation was modeled. Specifically, the variants were considered to form independently, yet the total fraction of all variants was considered at each computation time step in order apply the Avrami's extended space formulation correctly, where the probability of formation of new bainitic variants decreases with increased bainitic fraction in the system [15]. However, in this approach, the interactions between the variants are not taken into account. These interactions between the variants can indeed influence the distribution of the volumetric fraction of the active bainitic variants inside a grain, which may not be exactly the same as introduced herein, since the current model reflects an ideal case. It should be noted that the redistribution of the bainitic fractions of the variants may notably affect the resultant transformation strains in macroscale.

Another reason may be the formation of cementite in the parent phase during the transformation. As mentioned previously, this phenomena was not taken into account in the current model since the volumetric fraction of the cementite expected to form in the system may be ignored due to its low amount, and is beyond the scope of the current study, which focuses on the computation of isothermal kinetics curve and the corresponding transformation strains utilizing a single model. The original kinetics model [15] that constitutes the basis of the current model is applied to predict the general formation of bainite in the system, where the cementite precipitation is suppressed by high Si content. The current results indicate that the adaptation of this approach to the current model with the previously described modifications, where the formation is cementite is expected, yielded reasonable results.

Figures 19-22 below are the SEM-EBSD images of the specimens after the transformation in various load conditions. The figures are useful in terms of understanding the effect of stresses on the final texture.

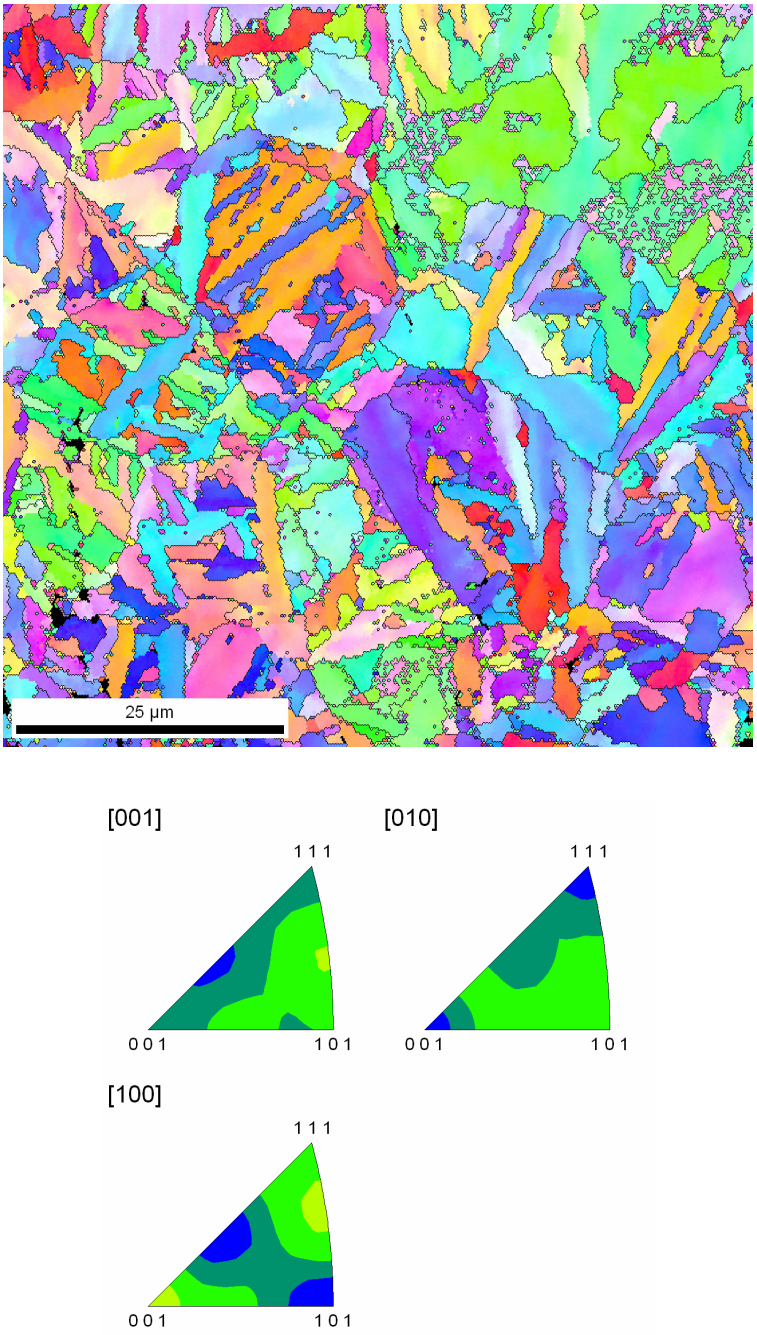

Figure 19: Transformed texture with no applied stress. A homogenous distribution of the orientations is visible.

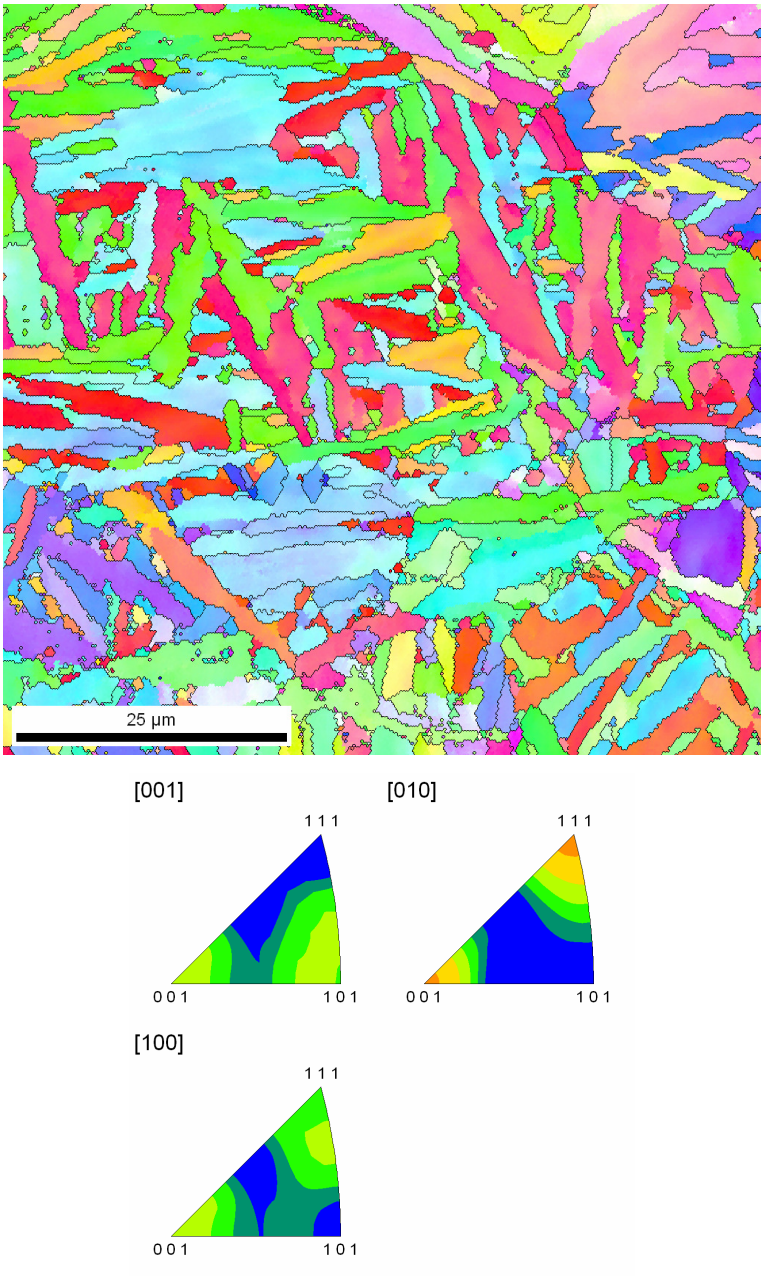

Figure 20: Transformed texture with 140 MPa tensile stress. Product phase forms with higher volumetric fraction in certain orientations.

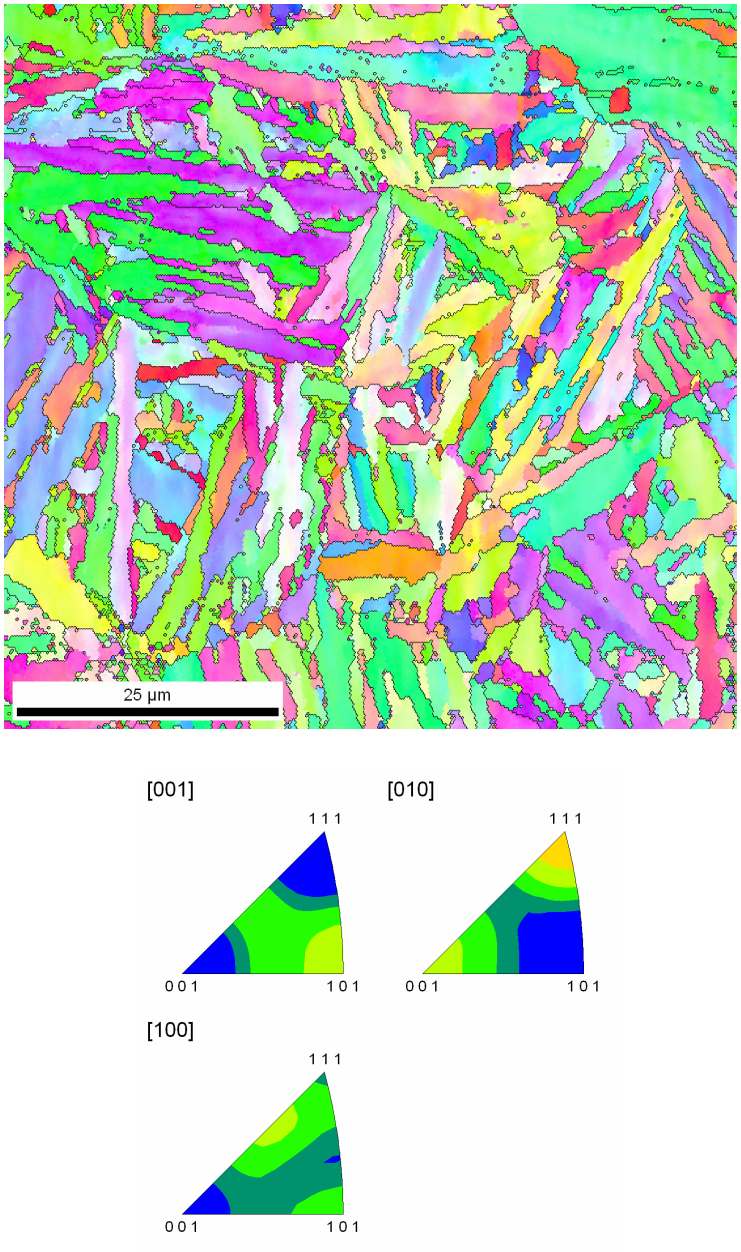

Figure 21: Transformed texture with 140 MPa compressive stress. Compared with 140 MPa tensile stress, it is seen that variants with different orientations are denser.

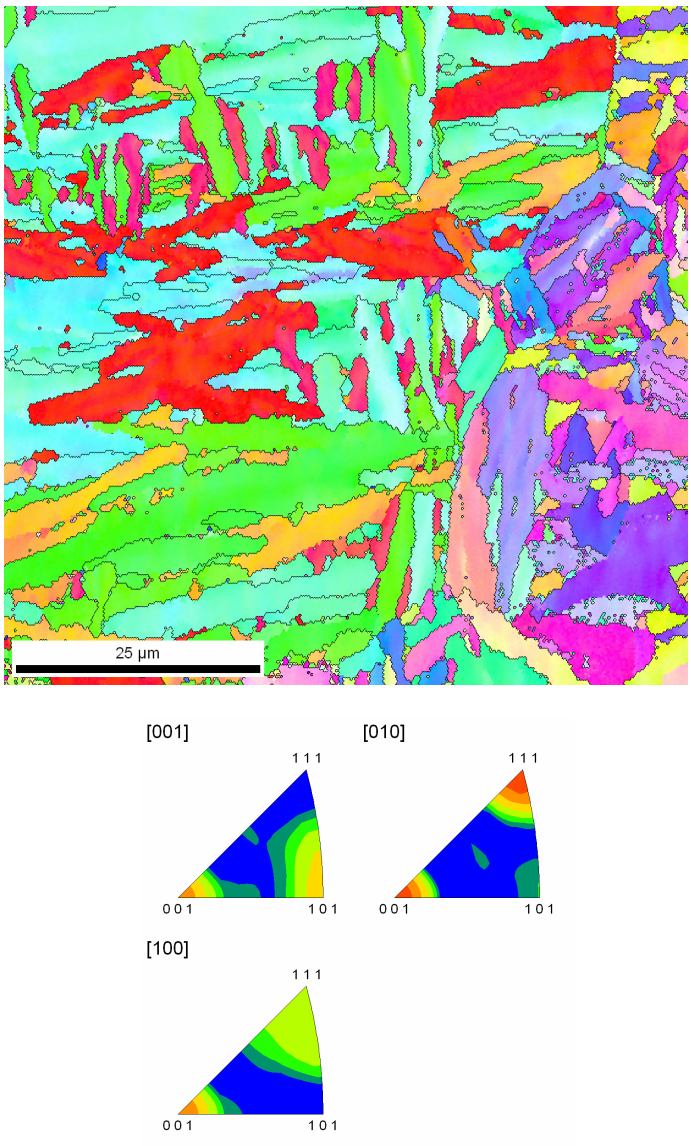

Figure 22: Transformed texture with 100 MPa tensile stress and 6% plastic pre-deformation. The effect of internal stresses introduced with the plastic deformation has remarkable effects on texture evolution and favors the formation of bainitic phase at certain orientations

Chapter 6

CONCLUSION AND FUTURE WORK

6.1) Conclusion

A variant based transformation kinetics approach was adopted to model both the isothermal bainitic transformation behavior and the corresponding transformation strains in a steel undergoing bainitic transformation under stress levels where the variant selection has remarkable effects on the transformation kinetics and the transformation strain anisotropy. Both the isothermal transformation kinetics curves and the resultant transformation strains are predicted correctly with a single formulation, where the MDF introduced due to the applied external stresses is distributed to the system and carry deviations from variant to variant.

Specifically, a model developed previously for a stress free transformation is modified in order to reflect the deviations in the nucleation rates of the variants under applied stresses [15]. The proposed model applies the same algorithm proposed for the growth of a sheaf to each bainitic variant. In stress free case, since all bainitic sheaves with different crystallographic orientations have the same nucleation rate, the formation of a single variant is enough to reflect the general isothermal kinetics, where the transformation strain field calculations would still need further modifications. Current model takes into account the varying nucleation rates of bainitic variants under stressed conditions, and gives the volumetric fraction of each bainitic variant at any instant through the transformation. The obtained volumetric fractions are further used in order to calculate the resultant transformation strain in macroscale. The model is remarkable in terms of obtaining the transformation kinetics and the resultant transformation strain fields simultaneously, due to its variant based approach.

6.2) Future Work

The proposed model predicted the experimentally determined kinetics and strain results with high accuracy. During the calculations, our approach carried certain simplifications and assumptions. Further improvements will make the model physically more complete.

A major improvement that shall be done is to model the formation of cementite through the transformation, ongoing simultaneously with bainitic ferrite formation. Formation of cementite is ignored in the current study, by assuming that the final volumetric fraction of cementite is negligible when compared with that of bainitic ferrite in the system. Even though that may be the case for the material studied, different chemical compositions may lead different final microstructures. Accordingly, additional kinetics formulations should be adopted to model the formation of cementite during the transformation. This improvement would make the applicability of the model possible to a wide range of materials. Besides cementite, formation of any additional phases should also be formulated, depending on the material.

The interaction energies between the bainitic variants aren't taken into account. The interaction energies between the bainitic variants will be more important in the cases with high number of variants active in the system, where higher number of variants mean higher resistance to the growth of sheaves. The interactions energies between the variants should be incorporated to the energy calculations.

The total strain of a grain in the bulk material due to the transformation strains of the bainitic variants inside is modeled by using the Eshelby tensor. Depending on the transformation strain results and the active variants obtained by fitting the simulation to the experimental data, it may be concluded that this approach had reasonable outcomes; however, the total strain field of the grain can be obtained with more detailed and specific calculations.

In the kinetics theory, the competitive growth of the bainitic variants may be modeled more accurately, by introducing additional terms reflecting the competitive growth of the variants, where an attempt is made by Rees and Shipway [16]. This requires detailed experimental data, specifically, EBSD-SEM studies are needed to obtain the density of variants upon transformation, to compare with the simulation results.

And finally, detailed experimental study is needed to understand the relation between the number of active variants in the system and the ratio of MDF to TDF. This would make the model independent from the experiments, since a fitting procedure to the experiment data will not be needed to finalize the simulation results.

BIBLIOGRAPHY

[1] Lambers, H-G, Tschumak, S, Maier HJ, Canadinc, D. Tensile Properties of 51 CrV4 Steel in Martensitic, Bainitic and Austenitic State. eds.: Oldenburg, M., Steinhoff, K., Prakash, B., 2 nd International Conference Hot Sheet Metal forming of high-performance steel CHS 2 , Verlag Wissenschaftliche Scripten, Lulea, Sweden; 2009. p. 77.

[2] Jacques PJ, Girault E, Harlet Ph, Delannay F. ISIJ Int 2001;41:1061.

[3] Takahashi M. Curr Opin Solid St M 2004;8:213.

[4] Garrett RP, Xu S, Lin J, Dean TA. Int J Mach Tool Manu 2004;44:831.

[5] Bhadeshia HKDH. Bainite in steels. 2nd ed.. IOM;2001. p. 345.

[6] Garcia-Mateo C, Caballero FG, Bhadeshia HKDH. Mater Sci Forum 2005;500:495.

[7] Bhadeshia HKDH. Bainite in steels. 2nd ed.. IOM;2001. p. 348.

[8] Caballero FG, Bhadeshia HKDH. Curr Opin in Solid S M 8;2004:251.

[9] Garcia-Mateo C, Caballero FG, Bhadeshia HKDH. ISIJ Int 2003;43:1238.

[10] Bhadeshia HKDH. Bainite in steels. 2nd ed.. IOM;2001. p. 353.

[11] Ohta A, Matsuoka K, Nguyen NT, Maeda Y, Suzuki N. Weld J Research Supplement 2003; 82:77

[12] Ohta A, Suzuki N, Maeda Y, Hiraoka K, Nakamura T. Int J Fatigue 1999;21:113

[13] Bhadeshia HKDH. Mater Sci Eng 2004;A378:34.

[14] Lambers HG, Tschumak S, Maier HJ, Canadinc D. Metall Mater Trans 2009;A40:1355.

[15] Matsuda H, Bhadeshia HKDH. Proc R Soc Lond 2004;A460:1707.

[16] Rees GI, Shipway PH. Mater Sci Eng 1997; A223:168.

[17] Davenport ES, Bain EC. Trans Met Soc AIME 1930;90:117.

[18] Bhadeshia HKDH. Bainite in steels. 2nd ed.. IOM;2001. p. 2.

[19] Bain EC, Alloying Elements in Steel, ASM, Cleveland, Ohio, USA 1939.

[20] Bhadeshia HKDH. Bainite in steels. 2nd ed.. IOM;2001. p. 3.

[21] Bhadeshia HKDH. Bainite in steels. 2nd ed. IOM;2001. p. 4.

[22] Vilella JR, Guelich GE, Bain EC. Trans ASM 1936;24:225.

[23] Bhadeshia HKDH. Bainite in steels. 2nd ed. IOM;2001. p. 5.

[24] Aaronson HI, Wells C. Trans AIME 1956;206:1216.

[25] Bhadeshia HKDH. Bainite in steels. 2nd ed.. IOM;2001. p. 19.

[26] Bhadeshia HKDH, Edmonds DV. Acta Metall Mater 1980;28:1265

[27] Oblak JM, Hehemann RF. Transformations and Hardenability in Steels. Climax Moly Ann Arbor 1967. p. 15.

[28] Hehemann RF, Kinsman KR, Aaronson HI. Metall Trans 1970;3:1077.

[29] Porter DA, Easterling KE. Phase Transformations in Metals and Alloys. Chapman & Hall London 1981. p. 382.

[30] Bhadeshia HKDH, Edmonds DV. Metall Trans 1979;A10:895.

[31] Bhadeshia HKDH. Bainite in steels. 2nd ed. IOM;2001. p. 129.

[32] Bhadeshia HKDH. Acta Metall Mater 1981;29:1117.

[33] Ali A, Bhadeshia HKDH. Mater Sci Technol 1989;5:398.

[34] Bhadeshia HKDH. Met Sci 1982;16:159.

[35] Bhadeshia HKDH. Bainite in steels. 2nd ed. IOM;2001. p. 132.

[36] Ali A, Bhadeshia HKDH. Mater Sci Technol 1990;6:781

[37] Bhadeshia HKDH. J Phys-Paris 1982;C4:443.

[38] Garcia-Mateo C, Bhadeshia HKDH. Mater Sci Eng 2004;A378:289.

[39] Rees GI, Bhadeshia HKDH. Mater Sci Technol 1992;8:985.

[40] Rees GI, Bhadeshia HKDH Mater Sci Technol 1992;8:994

[41] Bhadeshia HKDH, David SA, Vitek JM, Reed RW. Mater Sci Technol 1991;7:686.

[42] Shipway PH, Bhadeshia HKDH. Mater Sci Eng 1995;A201:143.

[43] Swallow E, Bhadeshia HKDH. Mater Sci Technol 1996;12:121.

[44] Bhadeshia HKDH. Hot Workability of Steels and Light Alloys-Composites eds.: H.J. McQueen, E.V. Konpleva, and N.D. Ryan. Canadian Institute of Mining, Minetrals and Petroleum, Montreal, Canada;1996. p. 543.

[45] Chatterjee S, Bhadeshia HKDH. Mater Sci Technol 2007;23:1101.

[46] Hase K, Garcia-Mateo C, Bhadeshia HKDH. Mater Sci Technol 2004:20;1499.

[47] Patel JR, Cohen M. Acta Metall 1953;1:531.

[48] Wechsler MS, Lieberman DS, Read TA. Trans AIME 1953;197:1503.

[49] Han HN, Suh DW. Acta Mater 2003;51:4907.

[50] Kundu S, Hase K, Bhadeshia HKDH. Proc R Soc Lond 2007;A463:2309.

[51] Lee SH, Kang JY, Han HN, OH KH, Lee HC, Suh DW. ISIJ Int 2005;45:1217.

[52] Quidort D, Brechet Y. Scripta Mater 2002;47:151.

[53] Luzginova NV, Zhao L, Wauthier A, Sietsma J. Mater Sci Forum 2005;500:419.

[54] Quidort D, Brechet YJM. Acta Mater 2001;49:4161.

[55] Bhadeshia HKDH, Abreu H, Kundu S. Int J Mater Res 2008;99:342.

[56] Bhadeshia HKDH, Kundu S, Abreu H. M. Microstructure and Texture in Steels. eds.: A. Haldar, S. Suwas, and D. Bhattacharjee. Springer (London);2009. p. 19.

[57] Ledbetter H, Dunn ML. Mater Sci Eng 2000;A285:180.

[58] Kocks UF, Tome CN, Wenk HR. Texture and Anisotropy. Cambridge University Press (Cambridge); 1998. p. 25.

[59] Kocks UF, Tome CN, Wenk HR. Texture and Anisotropy. Cambridge University Press (Cambridge); 1998. p. 16.

[60] Peultier B, Ben Zineb T, Patoor E. Mech Mater 2006;38:510.

[61] Khan AS, Huang S. Continuum Theory of Plasticity. John Wiley & Sons, Inc (New York); 1995. p.397.

[62] Azuma M, Fujita N, Takahashi M, Senuma T, Quidort D, Lung T. ISIJ Int 2005;45:221

[63] Kozeschnik E, Bhadeshia HKDH. Mater Sci Technol 2008;24:343.

[64] Avrami M. J Chem Phys 1939;7:1103.

[65] Avrami M. J Chem Phys 1940;8:212.

[66] Avrami M. J Chem Phys 1941;9:177.

[67] Jones SJ, Bhadeshia HKDH. Acta Mater 1997;45:2911.

Vita

Can Uslu was born in Istanbul, Turkey in 1985. He graduated from Istanbul Atatürk Fen Lisesi, Istanbul, Turkey in 2004. He received his B.Sc. degree in Mechanical Engineering from Koc University, Istanbul, Turkey in 2008. Since then, he has enrolled in Koc University Mechanical Engineering M.Sc. program. During his master studies, he focused on experimental and computational solid mechanics, specifically studied on the kinetics of bainitic phase transformations in steels and the resulting texture.